LEVEL II

SDAC-TR-76-14

EMPIRICAL m_b:M_s RELATIONS AT THE NEVADA TEST SITE WITH APPLICATIONS TO m_b-YIELD RELATIONS

R.R. Blandford, M.F. Tillman & D.P. Racine

Seismic Data Analysis Center

Teledyne Geotech, 314 Montgomery Street, Alexandria, Virginia 22314

20 April 1977

APPROVED FOR PUBLIC RELEASE; DISTRIBUTION UNLIMITED.

Sponsored by

The Defense Advanced Research Projects Agency (DARPA)

ARPA Order No. 2551

Monitored By

AFTAC/VSC

312 Montgomery Street, Alexandria, Virginia 22314

Unclassified
SECURITY CLASSIFICATION OF THIS PAGE (When Data Entered)

REPORT DOCUMENTATION PAGE

READ INSTRUCTIONS BEFORE COMPLETING FORM

(14) 1. REPORT NUMBER: SDAC-TR-76-14

2. GOVT ACCESSION NO.

3. RECIPIENT'S CATALOG NUMBER

(6) 4. TITLE (and Subtitle): EMPIRICAL m_b:M_s RELATIONS AT THE NEVADA TEST SITE WITH APPLICATIONS TO m_b-YIELD RELATIONS.

(9) 5. TYPE OF REPORT & PERIOD COVERED: Technical rept.,

6. PERFORMING ORG. REPORT NUMBER

(10) 7. AUTHOR(s): R.R. Blandford, M.F. Tillman, D.P. Racine

(15) 8. CONTRACT OR GRANT NUMBER(s): F08606-76-C-0004, VARPA Order-2551

9. PERFORMING ORGANIZATION NAME AND ADDRESS
Teledyne Geotech
314 Montgomery Street
Alexandria, Virginia 22314

10. PROGRAM ELEMENT, PROJECT, TASK AREA & WORK UNIT NUMBERS
VT/6709

11. CONTROLLING OFFICE NAME AND ADDRESS
Defense Advanced Research Projects Agency
Nuclear Monitoring Research Office
1400 Wilson Blvd.-Arlington, Virginia 22209

(11) 12. REPORT DATE: 20 April 1977

13. NUMBER OF PAGES: 63

14. MONITORING AGENCY NAME & ADDRESS (if different from Controlling Office)
VELA Seismological Center
312 Montgomery Street
Alexandria, Virginia 22314

15. SECURITY CLASS. (of this report): Unclassified

(12) 67p.

15a. DECLASSIFICATION/DOWNGRADING SCHEDULE

16. DISTRIBUTION STATEMENT (of this Report)

APPROVED FOR PUBLIC RELEASE; DISTRIBUTION UNLIMITED.

17. DISTRIBUTION STATEMENT (of the abstract entered in Block 20, if different from Report)

18. SUPPLEMENTARY NOTES

Author's Report Date. 11/08/76

19. KEY WORDS (Continue on reverse side if necessary and identify by block number)

Magnitude	M_s
Yield	Nevada Test Site
m_b	NTS

20. ABSTRACT (Continue on reverse side if necessary and identify by block number)

Measurements have been made of first-motion amplitude and of the period and amplitude of the second peak-to-trough excursion (termed the c phase) for short-period vertical P-wave signals from approximately 60 Nevada Test Site (NTS) explosions. They were recorded at the Long-Range Seismic Measurement (LSRM) and Seismic Data Collection System (SDCS) stations in Houlton, Maine (HNME), and Red Lake, Ontario (RKON). Almost all events selected were detonated in saturated tuff or rhyolite. Care was taken to avoid gross errors and to minimize effects of apparent minor perturbations of the waveforms,

CONT'

DD FORM 1 JAN 73 1473 EDITION OF 1 NOV 65 IS OBSOLETE

78 07 03 051

Unclassified
SECURITY CLASSIFICATION OF THIS PAGE (When Data Entered)

408 258

which cause zero-crossings, the so-called "false cycles".

The c-phase data are plotted as a function of M_S and are interpreted to show amplitude variations of several tenths in magnitude with respect to an M_S: yield curve with slope of 1.0. These amplitude variations are due independently to: (1) the influence of yield on corner frequency; (2) interference with the pP phase; and (3) geographic location within NTS. Several tenths of a second variation in period can also be traced to the above 3 causes. The variation with geographic location may be due to variation of the upper 2 km of structure at NTS or to multipathing and ray divergency because of more deeply seated structures.

In general the data supports the conclusion that the m_b: yield curve begins to bend significantly at approximately 200 kt, as predicted by the ω^2 granite reduced displacement potential (RDP) of von Seggern and Blandford. The curvature may not have been detected earlier at NTS due to scatter in the data from the three effects mentioned above. Another possibility shown in this report is that near the 1000-kt region the slope of log (c/T) versus log (yield) is closer to 1.0 than is the slope of log (c) versus log (yield).

The scatter of the data is greater at RKON than at HNME, presumably reflecting the greater variability of signals at regional distances and the shallow takeoff angles. Network averages of teleseismic stations would certainly show less scatter. Despite the greater amount of scatter in single-station data, we feel that the general trends are clear enough to support the conclusions reached. Use of single-station data is useful because there are fewer "hidden" effects of data selection.

EMPIRICAL m_b:M_S RELATIONS AT THE NEVADA TEST SITE WITH APPLICATION TO m_b-YIELD RELATIONS

SEISMIC DATA ANALYSIS CENTER REPORT NO.: SDAC-TR-76-14

AFTAC Project Authorization No.:	VELA T/6709/B/ETR
Project Title:	Seismic Data Analysis Center
ARPA Order No.:	2551
ARPA Program Code No.:	6F10
Name of Contractor:	TELEDYNE GEOTECH
Contract No.:	F08606-76-C-0004
Date of Contract:	01 July 1975
Amount of Contract:	$2,319,926
Contract Expiration Date:	30 June 1976
Project Manager:	Royal A. Hartenberger (703) 836-3882

P. O. Box 334, Alexandria, Virginia 22314

APPROVED FOR PUBLIC RELEASE; DISTRIBUTION UNLIMITED.

SDAC-TR-76-14
Overlay in report may be obtained from
Teledyne Geotech

ABSTRACT

Measurements have been made of first-motion amplitude and of the period and amplitude of the second peak-to-trough excursion (termed the c-phase) for short-period vertical P-wave signals from approximately 60 Nevada Test Site (NTS) explosions. They were recorded at the Long-Range Seismic Measurement (LSRM) and Seismic Data Collection System (SDCS) stations in Houlton, Maine (HNME), and Red Lake, Ontario (RKON). Almost all events selected were detonated in saturated tuff or rhyolite. Care was taken to avoid gross errors and to minimize effects of apparent minor perturbations of the waveforms, which cause zero-crossings, the so-called "false cycles".

The c-phase data are plotted as a function of M_S and are interpreted to show amplitude variations of several tenths in magnitude with respect to an M_S: yield curve with slope of 1.0. These amplitude variations are due independently to: (1) the influence of yield on corner frequency; (2) interference with the pP phase; and (3) geographic location within NTS. Several tenths of a second variation in period can also be traced to the above 3 causes. The variation with geographic location may be due to variation of the upper 2 km of structure at NTS or to multipathing and ray divergency because of more deeply seated structures.

In general the data supports the conclusion that the m_b: yield curve begins to bend significantly at approximately 200 kt, as predicted by the ω^2 granite reduced displacement potential (RDP) of von Seggern and Blandford. The curvature may not have been detected earlier at NTS due to scatter in the data from the three effects mentioned above. Another possibility shown in this report is that near the 1000-kt region the slope of log (c/T) versus log (yield) is closer to 1.0 than is the slope of log (c) versus log (yield).

The scatter of the data is greater at RKON than at HNME, presumably reflecting the greater variability of signals at regional distances and the shallow takeoff angles. Network averages of teleseismic stations would certainly show less scatter. Despite the greater amount of scatter in single-station data, we feel that the general trends are clear enough to support the conclusions reached. Use of single-station data is useful because there are fewer "hidden" effects of data selection.

TABLE OF CONTENTS

LIST OF FIGURES

LIST OF FIGURES (Continued)

LIST OF FIGURES (Continued)

LIST OF FIGURES (Continued)

LIST OF FIGURES (Continued)

INTRODUCTION

The purpose of this report is to examine in detail the variation of single-station, short-period P parameters derived from measurements of the Nevada Test Site (NTS) explosion signals at single stations (RKON and HNME) as a function of M_S. Because M_S is a well-determined function of yield (von Seggern, 1976), this study is equivalent to an examination of the variation as a function of yield. Effects at single stations may more clearly show effects of epicentral geology. As of this writing (October 1977), final computer outputs are combining the results in this paper with those from 3 other stations to produce network-average results. Preliminary results indicate little change in the qualitative conclusions.

Several other authors have already approached this problem. Among them are Marshall et al. (1971) and von Seggern (1976), who have discussed data which confirm simple cube-root scaling predictions of an M_S:log(yield) slope of 1.0. von Seggern (1976) found that M_S from the NTS explosions below the water table at Pahute Mesa were 0.1 and 0.2 magnitude units higher than M_S values for equivalent-yield shots below the water table elsewhere at NTS. von Seggern also pointed out that the scatter of the M_S:yield data points within regions at NTS is very small for events below the water table. He also showed, however, that if only pure teleseismic LR measurements in the range of 17 to 23 sec are used, then for corresponding yields (BOXCAR and MILROW), M_S is 0.5 units larger for explosions at NTS than at Amchitka. Since from each region these events fall on a very tight M_S:yield curve of slope 1.0, this discrepancy would apply to any pair of events, one at each test site.

The above findings show the importance of m_b:yield relationships for a threshold test-ban treaty. Despite controversy over the existence of m_b-magnitude bias at different test sites (Der, 1976), m_b bias is generally thought

---

von Seggern, D. H. (1976). M_S versus yield of underground nuclear explosions at the Nevada Test Site; SDAC-TR-76-11, Teledyne Geotech, Alexandria, Virginia.

Marshall, P. D., A. Douglas, and J. A. Hudson (1971). Surface waves from underground nuclear explosions; Nature, 234, 8-9.

Der, Z. A. (1976). On the existence, magnitude and causes of broad regional variations in body-wave amplitude (magnitude bias); SDAC-TR-76-8, Teledyne Geotech, Alexandria, Virginia.

to be less than 0.5 units ($0.1 < \text{bias} < 0.25$), and most workers accepting the existence of m_b bias also think it can be removed by careful attention to detailed corrections applied to the station magnitudes comprising network magnitude averages. Thus, m_b may be a more reliable estimate of yield than M_S, making m_b:yield relations worthy of more serious study.

Springer and Hannon (1973) presented m_b:yield data for explosions at Pahute Mesa. They concluded that the m_b:log(yield) slope is approximately 1.0 for teleseismic distances, and approximately 0.6 for regional distances. They attributed the difference to the total effect of absorption which increases with distance, and then they developed theoretical signal spectra which implied waveforms that would produce such a change of slope with distance.

Blandford (1976) computed observed regional spectral ratios for Pahute Mesa events ranging in magnitude from 0.7 to 1200 kilotons. Using the RAINIER reduced displacement potential (RDP) for tuff, he found that the spectral ratios and relative amplitudes agreed with the predictions of theory outlined by von Seggern and Blandford (1972). The same conclusion was reached by Noponen (1975) in comparing granite RDP to teleseismic observations of USSR and NTS explosions and by Lyuke et al. (1976) for regional observations of USSR explosions. Blandford, like Rodean (1972), calculated theoretical

---

Springer, D. L., and W. J. Hannon (1973). Amplitude-yield scaling for underground nuclear explosions; Bull. Seism. Soc. Am., 63, 477-500.

Blandford, R. R. (1976). Experimental determination of scaling laws for contained and cratering explosions; SDAC-TR-76-3, Teledyne Geotech, Alexandria, Virginia. DDC: ADA 03635.

von Seggern, D. H., and R. R. Blandford (1972). Source time functions and spectra for underground nuclear explosions; Geophys. J. R. Astr. Soc., 31, 83-97.

Noponen, I. (1975). Compressional wave power spectrum from seismic sources; Institute of Seismology, University of Helsinki, ISBN 951-45-0538-7, Contract AFOSR-72-2377 Final Report.

Lyuke, E. I., S. K. Daragan, and V. E. Peregontseva (1976). Forecasting the seismic wave spectra of large underground detonations from the spectra of small preliminary detonations; Phys. Solid Earth (from Izvestiya), 12(2), 103-109.

Rodean, H. C. (1972). Nuclear-Explosion Seismology; U.S. Atomic Energy Commission, Division of Technical Information, Oak Ridge, Tennessee.

waveforms and the associated m_b:yield curves. Using the tuff potential, Blandford found that absorption alone could not explain the near-unity m_b: yield teleseismic slope. He concluded that two RDP's calculated from measurements at angles of departure appropriate to regional and teleseismic distances could not be the same.

This report shows that the granite RDP does fit the NTS teleseismic data. von Seggern and Blandford (1972) and Blandford (1976), using first-motion data to avoid pP interference effects, detected the decrease in slope implied by the granite RDP for events LONGSHOT, MILROW, and CANNIKIN, detonated at Amchitka.

Mueller and Murphy (1971) obtained emprical scaling results for events as a function of depth that implied a fairly strong departure from pure cube-root scaling (variation of the RDP as a function of yield) as depth of the event changed. Note, however, that material properties of the medium varied with depth for many of the events used in their regression analyses to determine empirical factors. Using this theory, Murphy (1976) presented theoretical spectral ratios for the events REX and SCOTCH, which agree with his data. However, regional spectral data for these events presented by Blandford (1976) agreed with pure cube-root scaling, and disagreed with Murphy's data. A possible hypothesis for resolving the conflict in the experimental data is to assume large relative values of low-frequency earth noise for Murphy's low-magnitude REX event data, and equally high millimicron noise, due to high-frequency system noise, for his large-magnitude SCOTCH event. Blandford (1976) recognized and discussed such data-biasing effects. The effect of these noise biases on the SCOTCH/REX spectral ratio is to raise the ratio at low frequencies, and lower it at high frequencies. This difference is exactly that observed between the data presented by Blandford (1976) and the data of Murphy (1976). The theories of the two authors differ in the same way as do their data.

This report treats a greater volume of NTS data than was available to Springer and Hannon (1973) because it utilizes the Special Data Collection System (SDCS) data from stations RKON and HNME. Care is taken to

---

Mueller, R. A., and J. R. Murphy (1971). Seismic characteristics of underground nuclear detonations: Part I, Seismic spectrum scaling; Bull. Seism. Soc. Am., 61, 1675-1692.

measure at each station a common cycle for each event. This is accomplished by tracing each signal and picking the cycle while all the data are displayed for comparison. Many potential gross data errors, seemingly inevitable in projects of this size, were removed by careful reexamination of the original waveforms and calibration logs when plots of the data revealed outlying points. The data have been stored in a computer file and plots are produced by computer.

EVENT SELECTION AND MEASUREMENTS

Events selected for study are listed in Table I. In general they consist of explosions with yields greater than about 10 kt (HANDCAR, 12kt, and HARDHAT, 5.9 kt, are among the smaller events) and detonated below the water table. Several events from above the water table are included, but are within a 1-cavity radius of the water table. Also included are events at Ranier Mesa that are above the water table, but are thought to be in or near layers of perched water (Ramspott and Howard, 1975). A few events well above the water table are included because: (1) either they are events with shot reports prepared using the SDCS (EDAM, MARCH); (2) they are in dolomite (HANDCAR, KANKAKEE); or (3) they are of special interest for other reasons (DURYEA, MING VASE).

Most of the data in Table I are taken from Springer and Kinnaman (1971). Data for events after 1970 have been taken from data synopsis sheets that the U.S. Energy Research and Development Agency (ERDA) issued for each of the recent tests. For several of these reports, the average sound velocity from shot-point to surface was estimated by vibroseis or similar technique. It is these values which are reported in Table I. For events before 1970, the average values for each region (Pahute Mesa, 2.9 km/sec; Ranier Mesa, 2.6 km/sec; Yucca Flats, 1.7 km/sec) reported by Ramspott and Howard (1975) were used. Exceptions were made in the case of dolomite and granite, which used velocities of 2.7 and 5.5 km/sec, respectively. The average regional values are approximations, and though they probably should not be used for detailed comparison of individual predictions with observations, they may be adequate for the predominantly statistical conclusions reached in this study. The symbol for each event (see Table I) is the same as plotted on the map (Figure 1), showing the relative positions of the events. Small perturbations have been made in the locations of a few events at Yucca Flats so their symbols would not overlap, but their relative positions have been

Ramspott, L. D., and N. W. Howard (1975). Average properties of nuclear test areas and media at the USERDA Nevada Test Site; UCRL-51948, Lawrence Livermore Laboratory, Livermore, California.

Springer, D. L. and R. L. Kinnaman (1971). Seismic source summary for U.S. underground nuclear explosions, 1961-1970; Bull. Seism. Soc. Am., 61, 1073-1098.

TABLE I

SYMBOL	NAME	DATE	LATITUDE	LONGITUDE	DEPTH SHOT (M)	DEPTH WATER TABLE (M)	YIELD	RG	MS	VEL
0	Bilby	130963	37.060N	116.022W	798.8	545.3	235.0	YU	4.66	1.7
1	Handcar	51164	37.174N	116.067W	449.5	664.6	12.0	YU	3.00	2.7
2	Wagtail	30365	37.065N	116.037W	838.0	569.1	----	YU	3.73	1.7
3	Corduroy	31265	37.165N	116.052W	762.0	633.9	----	YU	4.04	1.7
4	Lampblack	180166	37.092N	116.019W	627.8	632.2	----	YU	----	1.7
5	Rex	240266	37.272N	116.434W	751.1	717.4	16.0	PM	3.50	2.9
6	Duryea	140466	37.243N	116.431W	608.7	739.5	65.0	PM	3.95	2.9
7	Chartreuse	60566	37.348N	116.322W	744.0	745.7	70.0	PM	3.99	2.9
8	Piranha	130566	37.087N	116.033W	613.4	596.4	----	YU	4.05	1.7
9	Dumont	190566	37.111N	116.058W	749.8	613.4	----	YU	3.91	1.7
A	Tan	30666	37.068N	116.035W	626.7	572.5	----	YU	4.00	1.7
B	Double Play	150666	37.060N	116.203W	366.4	344.2	----	SM	----	1.7
C	Kankakee	150666	37.172N	116.049W	509.2	642.4	----	YU	3.55	2.7
D	Halfbeak	300666	37.316N	116.293W	916.1	720.8	300.0	PM	5.06	3.3
E	Greeley	201266	37.302N	116.408W	1358.1	688.4	825.0	PM	5.36	2.9
F	Nash	190167	37.144N	116.135W	406.9	415.8	----	YU	3.70	2.4
G	Bourbon	200167	37.100N	116.004W	625.7	671.4	----	YU	3.98	1.7
H	Agile	230267	37.127N	116.066W	817.9	630.5	----	YU	4.22	1.7
I	Commodore	200567	37.130N	116.064W	834.6	633.9	250.0	YU	4.59	1.7
J	Scotch	230567	37.275N	116.370W	1092.9	753.2	150.0	PM	4.51	2.9
K	Knickerbocker	260567	37.248N	116.480W	705.1	707.2	71.0	PM	4.18	2.9
L	Midi Mist	260667	37.202N	116.208W	419.2	512.9	----	RM	3.14	2.6
M	Door Mist	310867	37.178N	116.209W	498.6	1022.4	----	RM	3.07	2.6
N	Zaza	270967	37.099N	116.053W	745.7	598.1	----	YU	4.17	1.7
O	Lanpher	181067	37.116N	116.058W	798.5	616.8	----	YU	4.29	1.7
P	Cobbler	81167	37.092N	116.036W	749.8	621.6	----	YU	3.18	1.7
Q	Knox	210268	37.117N	116.054W	721.1	613.4	----	YU	4.28	1.7
R	Dorsal Fin	290268	37.185N	116.221W	458.4	969.6	----	RM	3.40	2.6
S	Stinger	220368	37.333N	116.311W	746.7	715.7	----	PM	4.33	2.9
T	Boxcar	260468	37.295N	116.456W	1295.0	675.5	1200.0	PM	5.58	2.9
U	Rickey	150668	37.265N	116.315W	764.1	797.5	----	PM	4.75	2.9
V	Chateaugay	280668	37.246N	116.493W	678.9	707.2	120.0	PM	4.23	2.9
W	Sled	290868	37.250N	116.347W	815.5	769.5	----	PM	4.45	2.9
X	Noggin	60968	37.136N	116.047W	650.6	623.7	----	YU	4.62	1.7
Y	Hudson Seal	240968	37.205N	116.206W	372.2	1022.4	----	RM	3.15	2.6
Z	Crew	41168	37.130N	116.087W	674.8	647.5	----	YU	----	1.7
a	Ming Vase	201168	37.010N	116.206W	344.2	545.3	----	SM	2.65	1.7
b	Benham	191268	37.231N	116.474W	1567.7	717.4	1100.0	PM	5.48	2.9
c	Wineskin	150169	37.209N	116.225W	579.4	988.3	----	RM	3.85	2.6
d	Cypress	120269	37.169N	116.211W	460.1	988.3	----	RM	----	2.6

TABLE I (Continued)

SYMBOL	NAME	DATE	LATITUDE	LONGITUDE	DEPTH SHOT(M)	DEPTH WATER TABLE(M)	YIELD	RG	MS	VEL
e	Blenton/Thistl	300469	37.082N	116.014W	623.3	618.6	----	YU	----	1.7
f	Purse	70569	37.283N	116.501W	669.3	664.6	----	PM	4.71	2.9
g	Jorum	160969	37.314N	116.461W	1295.0	637.3	----	PM	5.34	2.9
h	Pipkin	81069	37.257N	116.441W	690.1	719.1	----	PM	----	2.9
i	Calabash	291069	37.143N	116.064W	698.6	640.7	110.0	YU	4.23	1.7
j	Diesel Train	51269	37.180N	116.211W	468.6	1175.8	----	RM	----	2.6
k	Diana Mist	110270	37.201N	116.205W	446.4	1083.7	----	RM	----	2.6
l	Shaper	230370	37.086N	116.021W	626.7	613.4	----	YU	----	1.7
m	Handley	260370	37.300N	116.534W	1348.5	432.8	----	PM	5.45	2.0
n	Mint Leaf	50570	37.217N	116.184W	453.3	1010.5	----	RM	----	2.6
o	Tijeras	141070	37.071N	116.005W	626.7	606.6	----	YU	----	1.7
p	Carpetbag	171270	37.129N	116.083W	739.9	644.1	220.0	YU	----	1.7
q	Topgallant	280275	37.106N	116.056W	797.5	576.0	----	YU	----	1.7
r	Cabrillo	70375	37.134N	116.084W	671.0	633.9	----	YU	----	1.7
s	Dining Car	50475	37.188N	116.214W	428.4	1099.1	----	RM	----	2.6
t	Edam	240475	37.116N	116.087W	459.4	637.3	----	YU	----	1.7
u	Obar	300475	37.109N	116.029W	636.3	582.4	----	YU	----	1.7
v	Tybo	140575	37.221N	116.474W	855.4	704.4	----	PM	5.00	2.3
w	Stilton	30675	37.340N	116.523W	818.6	304.0	----	PM	4.55	2.2
x	Mizzen	30675	37.095N	116.036W	712.3	576.0	----	YU	4.30	1.5
y	Mast	190675	37.350N	116.320W	1018.7	744.6	----	PM	4.84	3.9
z	Camembert	260675	37.279N	116.369W	1465.8	747.0	----	PM	5.18	2.9
!	Marsh	60975	37.024N	116.028W	477.5	536.8	----	YU	----	1.4
"	Husky Pup	241075	37.222N	116.180W	389.2	0.0	----	RM	----	2.6
#	Kasseri	281075	37.290N	116.412W	1414.3	702.0	----	PM	5.32	3.0
$	Inlet	201175	37.225N	116.368W	915.7	786.2	----	PM	4.10	3.0
%	Leyden	261175	37.117N	116.019W	364.7	685.3	----	YU	----	1.4
&	Chiberta	201275	37.128N	116.062W	800.5	599.5	----	YU	4.42	1.8
(	Shoal	261063	39.200N	118.380W	410.7	3.4	12.0	FN	2.94	5.5
)	Piledriver	20666	37.227N	116.056W	517.3	3.4	56.0	CS	4.05	5.5
=	Hardhat	150262	37.226N	116.059W	321.4	3.4	5.9	CS	3.01	5.5
-	Muenster	30176	37.297N	116.333W	1623.6	755.9	----	PM	4.96	2.9
[	Keelson	40276	37.069N	116.030W	715.7	556.9	----	YU	4.33	1.7
+	Esrom	40276	37.107N	116.038W	732.4	584.8	----	YU	4.03	1.7
@	Fontina	120276	37.271N	116.488W	1362.9	665.2	----	PM	5.18	2.9
]	Chesire	140276	37.243N	116.420W	1304.9	699.0	----	PM	4.92	3.2
<	Estuary	90376	37.310N	116.498W	971.6	701.0	----	PM	4.93	2.7
>	Colby	140376	37.306N	116.471W	1423.5	637.3	----	PM	5.28	2.8
?	Pool	170376	37.256N	116.329W	982.9	771.6	----	PM	4.03	2.9
:	Strait	170376	37.107N	116.053W	672.1	565.7	----	YU	4.39	1.7

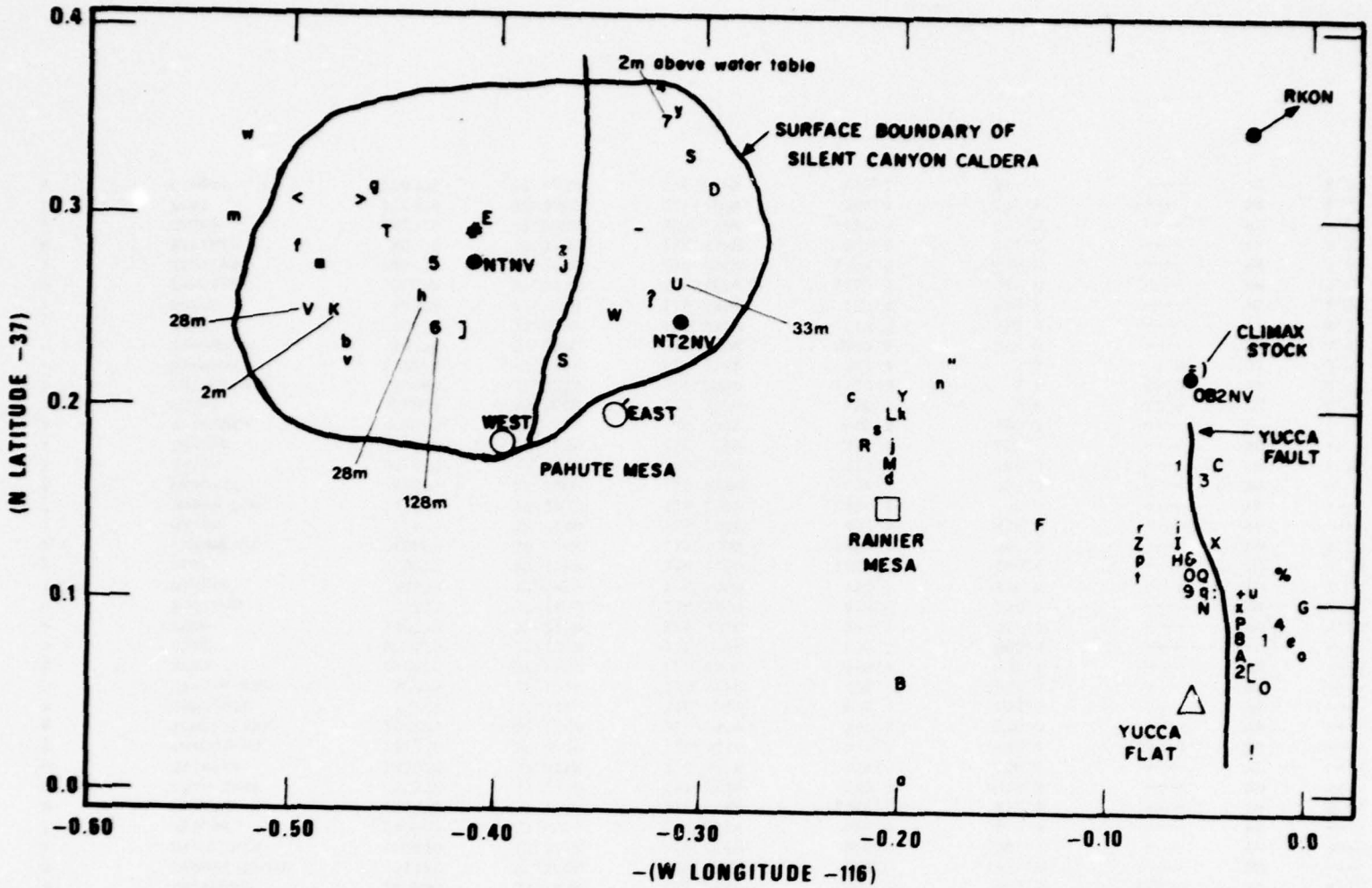

Figure 1. Locations of events discussed in this report at the Nevada Test Site. Events are indicated by numbers, upper and lower case letters, and other common symbols. The event associated with each symbol is given in Table I. Symbols for source regions are indicated, as well as azimuth to RKON. The outline of the Silent Canyon Caldera, as found by Orkild et al. (1969), is drawn around the Pahute Mesa events; and the surface trace of Yucca Fault, as mapped by Fernald et al. (1969), is drawn through the Yucca Flats events. Height above the water table is indicated in meters for the non-RAINIER events above the water table.

maintained. For example, if event A is east of event B on the ground, it is also east of event B on the map. Figure 1 is also included as a transparent overlay in the envelope attached at the back of this report.

Figure 2 gives the definitions of the measurements a, b, and c, made for this study. Note that the definition for measurement c is one swing later than what is used in most other studies. This definition was chosen so it more fully reflected the influence of pP. In almost every case, this c measurement is also equal to the maximum peak-to-trough measurement in the first 4 cycles used for calculating m_b. Note in Figure 2 how "false cycles" are ignored in making the measurements of c and T at HNME and RKON for event CAMEMBERT. The period T for the c measurements is defined as the interval between zero-crossings on either side. Note that at HNME, the c measurement gives close to the maximum amplitude in the signal, but at RKON for KASSERI the maximum amplitude occurs 4 cycles into the record. (The RKON signals vary substantially in character as a function of epicentral location and many look more like signals at HNME, which have a simple shape for all events.) Though these maximum amplitudes have been measured routinely in this study, they are ignored in order to analyze portions of the signal that may be predicted with planar, parallel-layer earth models: these 4- to 6-sec late arrivals may correspond to triplications or to mantle-multipaths that cannot presently be predicted. Measurements were also made for stations WH2YK and FNWV, and they have been included in the data base. However, the data are sparse because, unlike HNME and RKON, the stations WH2YK and FNWV were out of operation for long periods; therefore, measurements from those 2 stations have not been analyzed.

Figures 3a through 3f (from Blandford, 1976) show the variation of first motion (labelled "a"), the maximum peak-to-trough amplitude (labelled "c"), and the maximum peak-to-trough amplitude divided by period and corrected for system response at that period (labelled "c/T, corrected for instrument response") as a function of yield, for several values of the absorption parameter $t^* = T/Q$, where T is the travel time and Q is the average quality factor along the path. The RDP used in Figures 3a,b,c is for granite (von Seggern and Blandford, 1972) and varies as a function of yield. Although this potential is, strictly speaking, for granite and not for tuff, which is more

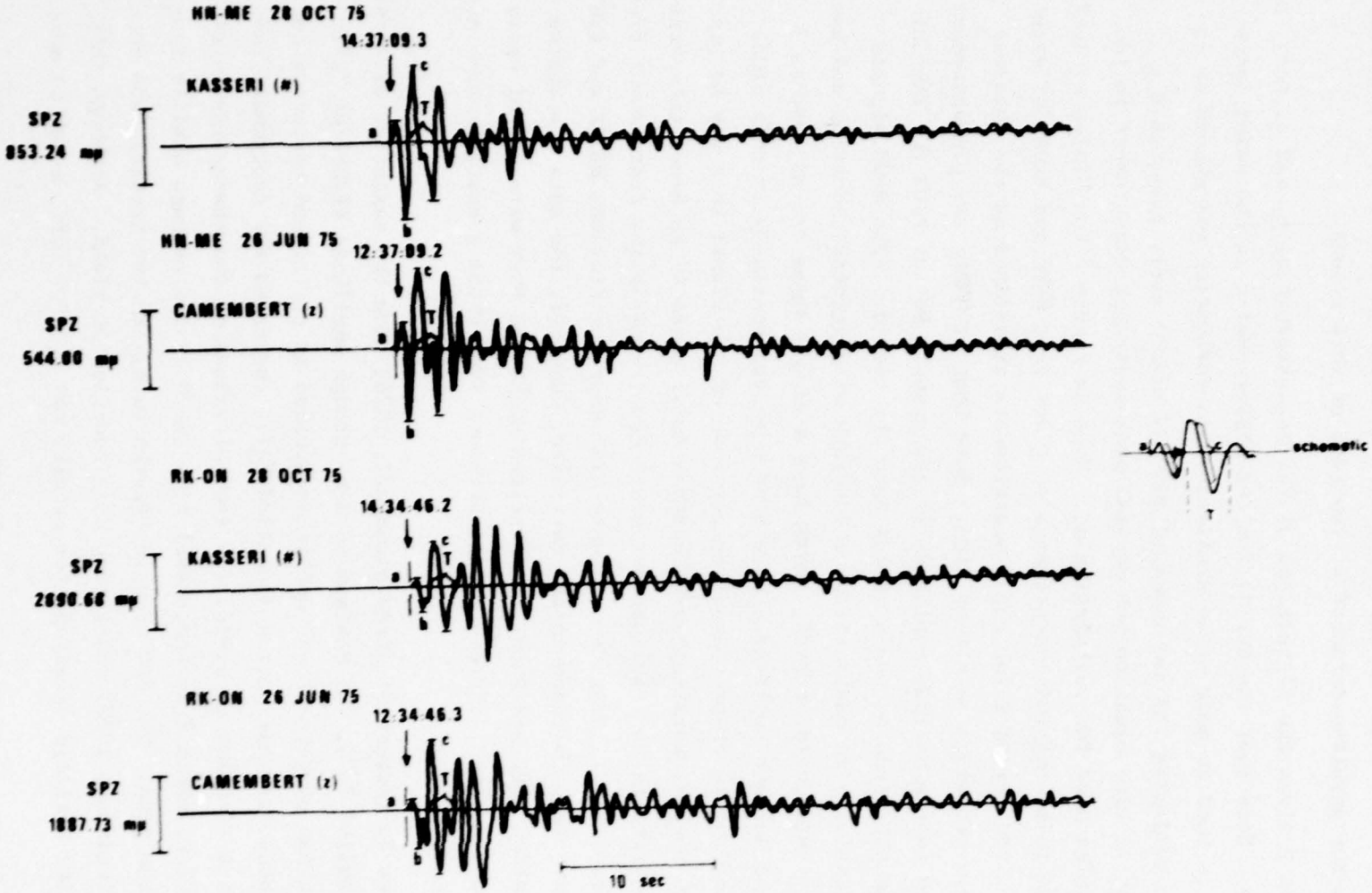

Figure 2. Waveforms of the events CAMEMBERT (z) and KASSERI (#) as seen at HNME and RKON. Measurements a, b, and c are indicated. For reasons discussed in the text, the definition for c is one-half cycle later than that usually used. Note that small, high-frequency "false cycles" are ignored in measurements of both amplitude and period.

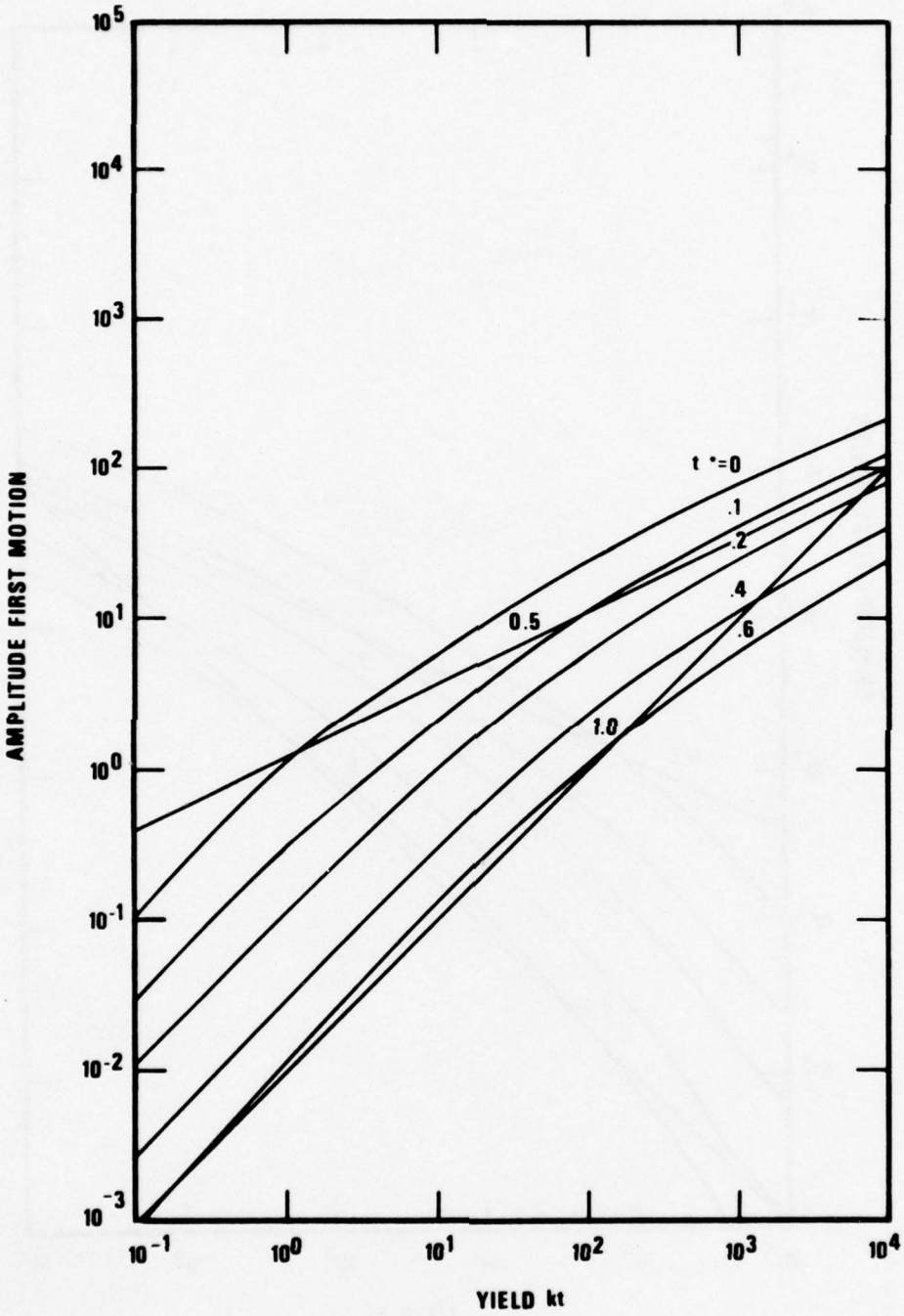

Figure 3a. Theoretical amplitude-yield curves for t* = 0, 0.1, 0.2, 0.4, 0.6; granite, amplitude of first motion, with no surface reflection. From Blandford (1976).

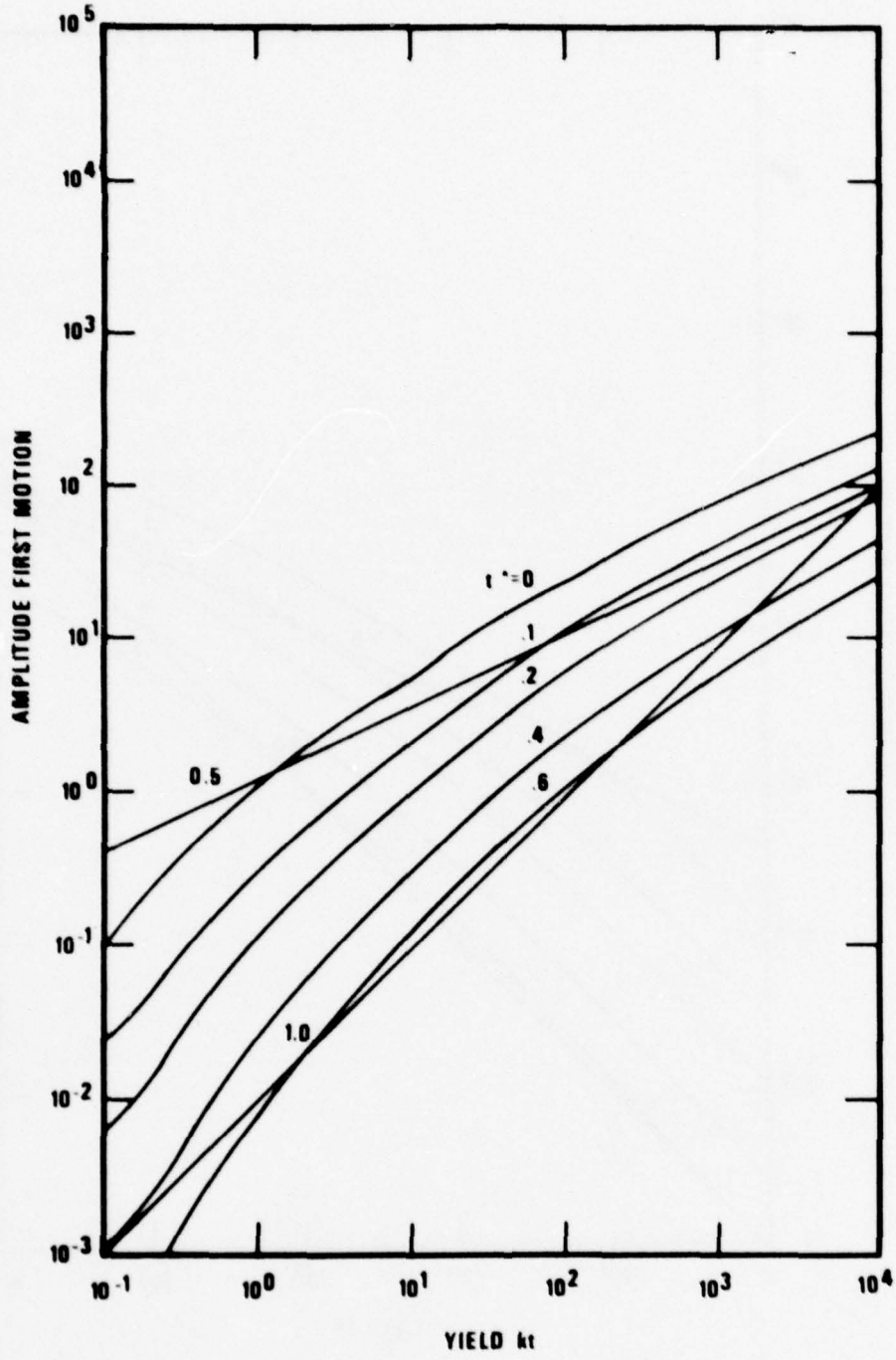

Figure 3b. Theoretical amplitude-yield curve for t* = 0, 0.1, 0.2, 0.4, 0.6; granite, amplitude of first motion, with surface reflection. pP delay equal to $0.12Y^{1/3}$ sec, with Y in kt. From Blandford (1976).

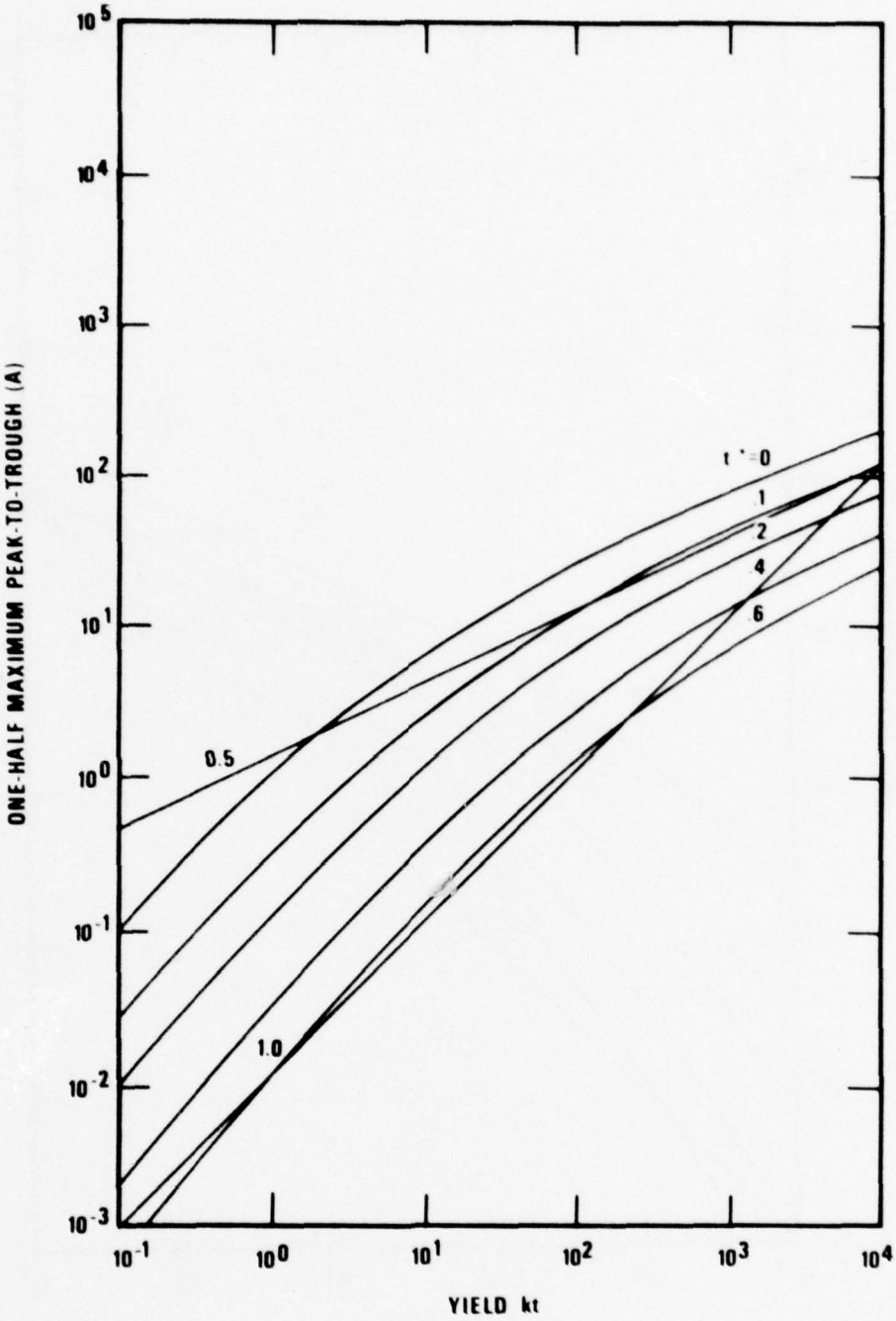

Figure 3c. Theoretical amplitude-yield curves for t* = 0, 0.1, 0.2, 0.4, 0.6; granite, one-half maximum peak-to-trough amplitude of signal, with no surface reflection. From Blandford (1976).

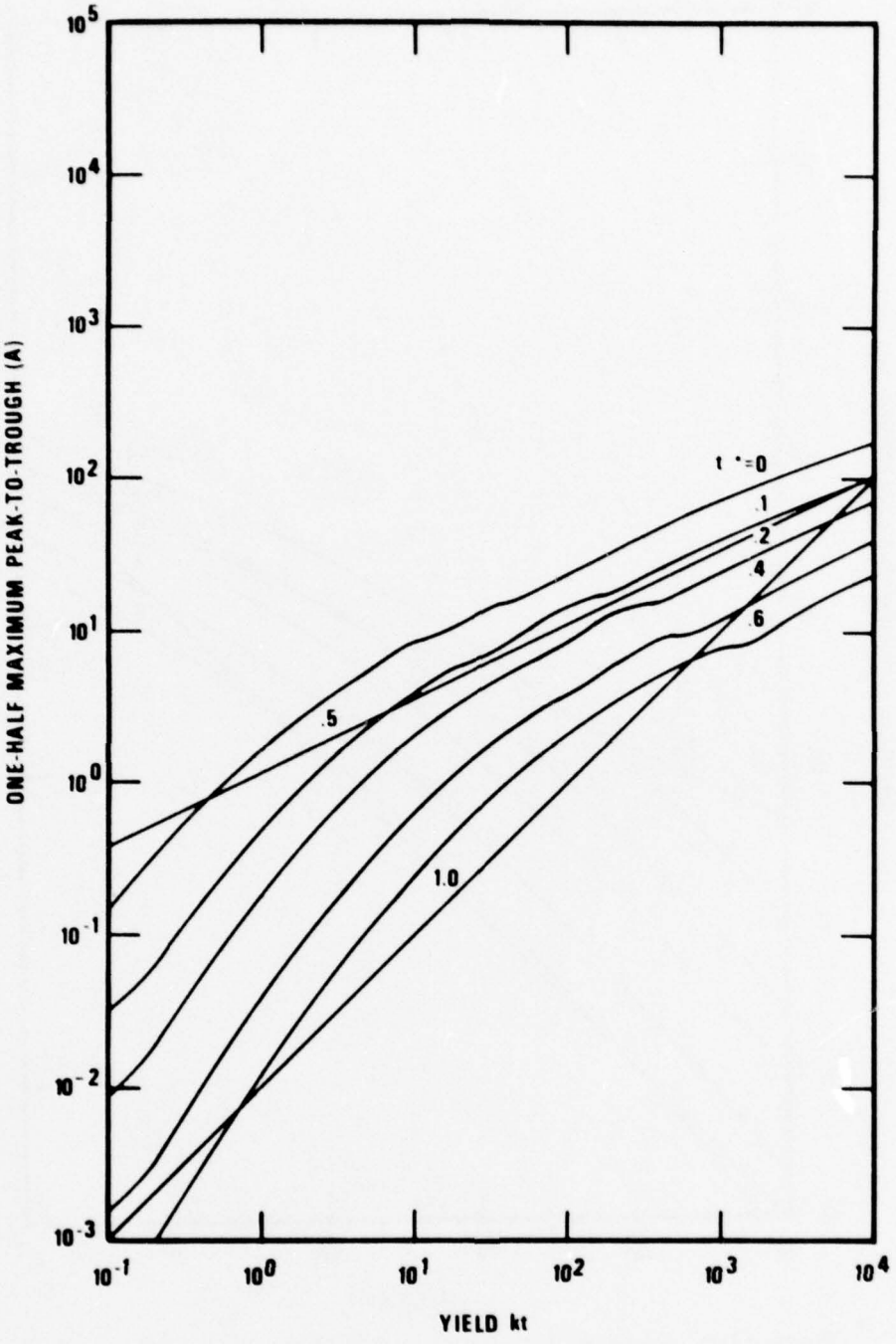

Figure 3d. Theoretical amplitude-yield curves for t* = 0, 0.1, 0.2, 0.4, 0.6; granite, one-half maximum peak-to-trough amplitude of signal, with surface reflection. pP delay equal to $0.12Y^{1/3}$ second, with Y in kilotons. From Blandford (1976).

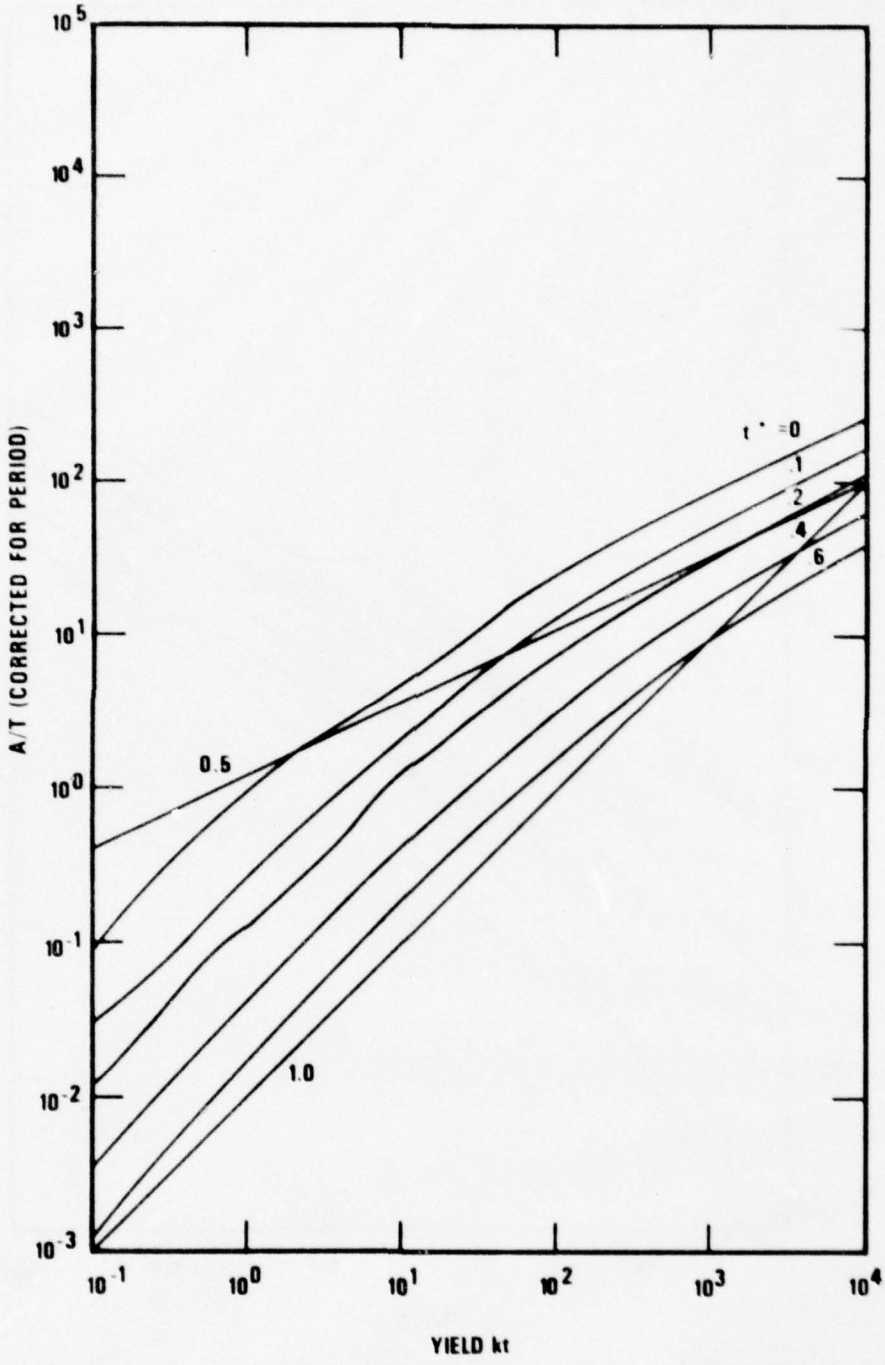

Figure 3e. Theoretical amplitude-yield curves for t* = 0, 0.1, 0.2, 0.4, 0.6; granite, one-half maximum peak-to-trough amplitude of signal, corrected for instrument response at measured period, T, and divided by T; with no surface reflection. From Blandford (1976).

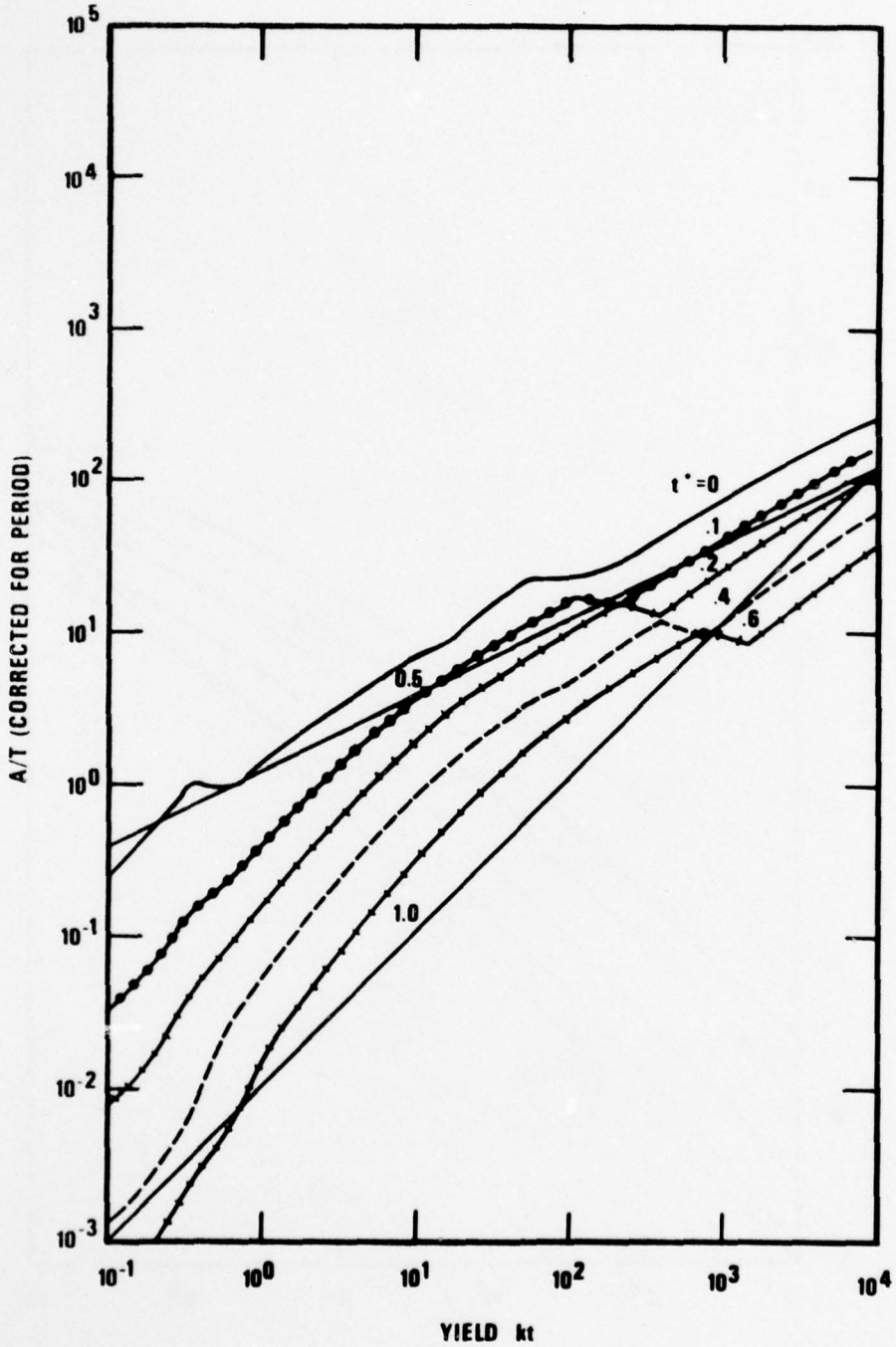

Figure 3f. Theoretical amplitude-yield curves for t* = 0, 0.1, 0.2, 0.4, 0.6; granite, one-half maximum peak-to-trough amplitude for signal, corrected for instrument response at measured period, T, and divided by T, with surface reflection. pP delay equal to $0.12Y^{1/3}$ sec, with Y in kt. From Blandford (1976).

typical of NTS, many workers such as von Seggern and Blandford (1972), Noponen (1975), Lyuke et al. (1976), have found it valid, as far as spectral shape is conerned, for several different types of competent, saturated rock observed at teleseismic distances. Blandford (1976) concluded that although tuff potential derived from RAINIER was satisfactory for observations at KNUT and MNNV 2 to 3 degrees away, it was inadequate for explaining teleseismic observations, implying that the RDP was a function of take-off angle. In this study, the granite potential is sufficient to explain teleseismic observations of explosions in saturated tuff.

Figures 3a, c, and e give results for the case where theoretically there is no free-surface reflection (pP). This could occur, for example, if the free surface were significantly "rough" or if there were significant spalling, resulting in "trapping" the pP signal. Figures 3b, d, f give results for the case in which, in theory, there is perfect free-surface reflection. In this case, a theoretical expression must be found for the reflection delay time, given by twice the depth divided by the average velocity. Assuming a velocity of 2.75 km/sec, and a containment depth formula (Y in kt) of $h = 0.16Y^{1/3}$ km, yields $\tau = 0.12Y^{1/3}$ sec. Many events at Yucca have delays more in accordance with $0.2Y^{1/3}$, while shots in granite, such as PILEDRIVER and HARDHAT, are more like $0.05Y^{1/3}$. Observed data should lie between the curves for perfect reflection and no reflection. Blandford (1976) concluded that the reflection coefficient for pP at NTS for frequencies greater than 0.5 Hz was between 0.5 and 0.2. Therefore, in this study, the experimental amplitude data is compared to Figures 3a, c, e, which neglect the effect of pP.

ANALYSIS OF RKON AND HNME DATA

RKON

Figure 4a shows a plot of the base-10 logarithm of RKON a-phase amplitude versus M_S from von Seggern (1976). For the smallest events, von Seggern used MNNV to determine M_S. For larger events, and for events after the 1970 closing of MNNV as an LRSM station, von Seggern used RKON. Data points are missing for several events after 1970 because: (1) the LR was too weak to be measured at RKON; (2) because the RKON short-period data was unavailable; or (3) because the RKON first-motion amplitude was judged to be severely contaminated by noise.

Figure 4a also includes the least-squares line with fixed slope of 1.0. Figure 4b shows a plot of the residuals derived from Figure 4a. This is standard procedure in this paper, except when plotting period T versus M_S, in which case both the slope and intercept are estimated. Reference to Figure 1 (use transparent overlay) and Table I will identify which event is plotted at each point in Figure 4b. If the magnitude residual lies between -0.1 and +0.1, then a "0" is plotted on Figure 4b. If the residual is 0.1 to 0.2, a "1" is plotted; if 0.2 to 0.3, a "2"; etc. If the residual is -0.1 to -0.2, then an "A" is plotted on Figure 4b. If the residual is -0.2 to -0.3, a "B"; etc. Note that in Figure 4b, the amplitudes from events in the western three-quarters of Pahute Mesa are substantially smaller than the amplitudes from events in the rest of NTS. Amplitudes from events in the eastern one-quarter are also smaller than those from the rest of NTS, but not by as great a margin. For this reason, Pahute Mesa is divided into two regions: the western region, for whose events the symbols are plotted within with an open circle (0); and the eastern region, where events are plotted within an open circle with a stick at "2 o'clock". Events shot at Rainier Mesa are plotted within a square (□) and events shot at Yucca Flats are plotted within a triangle (Δ).

In Figure 4a, there are also plotted two curves of the logarithm of first-motion amplitude versus yield; these are from Figure 3a, with $t^* = 0.4$. The upper line represents the data of Rainier Mesa and Yucca Flats and the lower line represents the Western Pahute Mesa data.

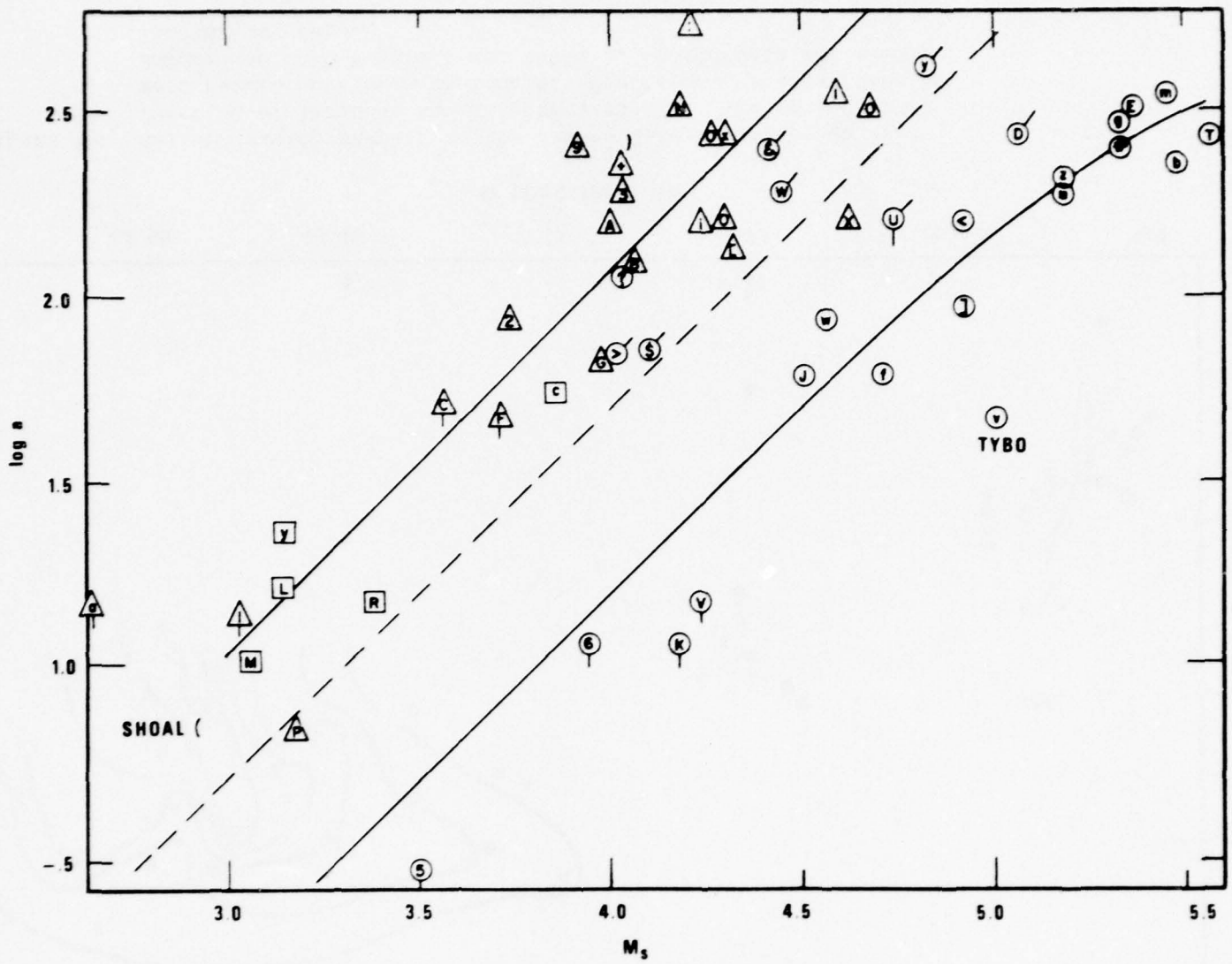

Figure 4a. RKON Station: Log (a) as a function of M_s. The dashed line is the least-squares line of slope 1.0 through all the data. The solid lines are from Figure 3a with t* = 0.4, with each line vertically adjusted by eye so they respectively best fit the west Pahute data and all other data.

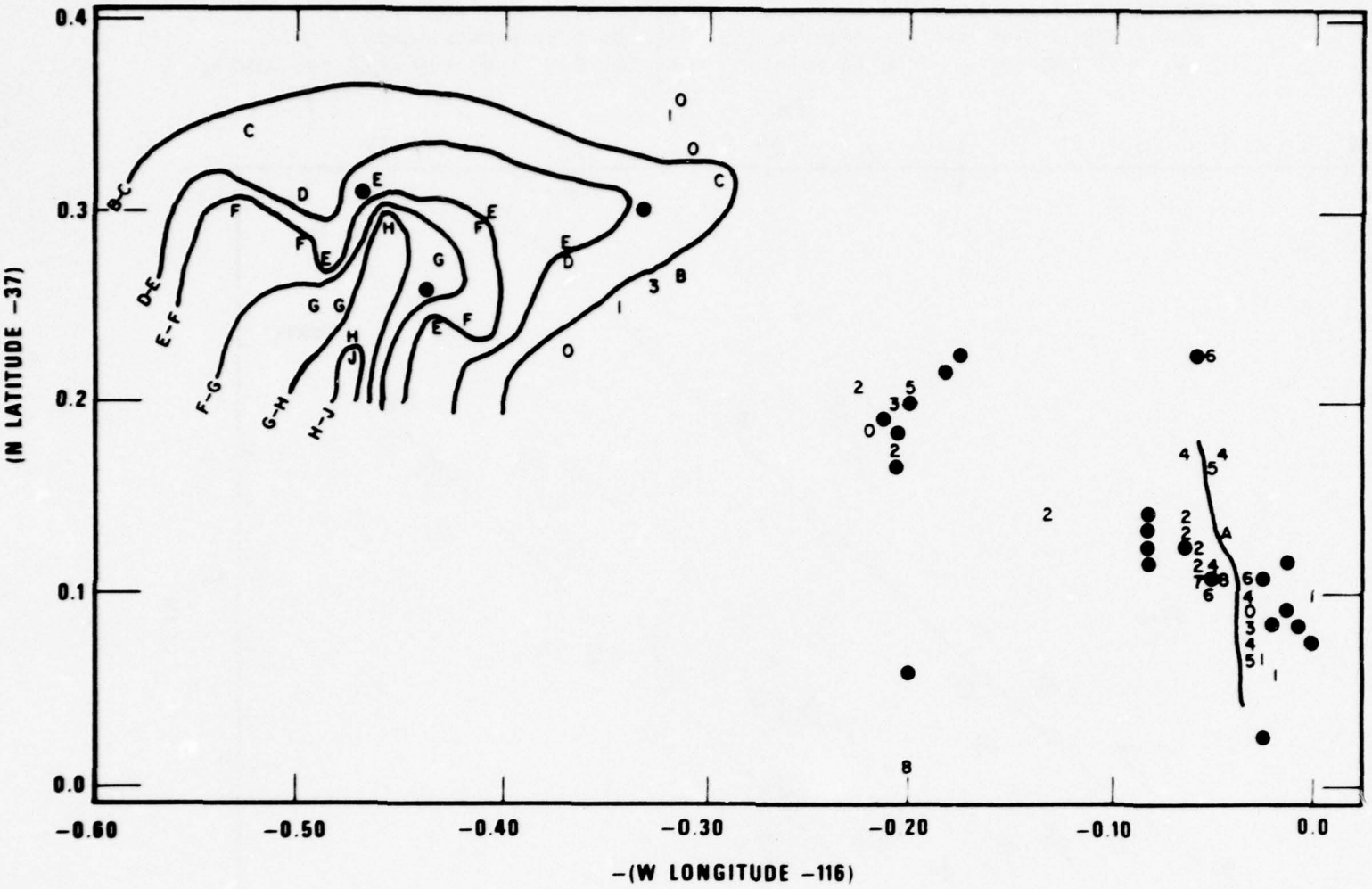

Figure 4b. Residuals with respect to the dashed line in Figure 4a as a function of latitude and longitude at NTS. The residuals at West Pahute have been contoured. Events may be identified by comparison with Figure 1 and Table I. Solid dots are events lacking any data.

The t* value is close to the value determined by Der and McElfresh (1976) for the NTS-RKON path.

The solid line trending north-south through Yucca Flats in Figure 4b represents the surface trace of Yucca Fault, taken from detailed geologic maps (Johnson and Hibbard, 1957; or Fernald et al., 1968). Fernald's map shows that the hard rock at Yucca Flats is covered by a layer of superficial deposits varying in depth from 700 m near COMMODORE (I) to 0 m near BOURBON (G).

To explain the large variance in residuals at Yucca, velocity and density profiles are used for the event OBAR, together with a Haskell matrix approach. Results show that for an event just below the surficial deposits -- paleozoic interface, the teleseismic amplitude may be reduced by a factor of 2 or more by cancelling the direct wave by the "internal pP" wave reflected from the interface. To determine if this type of calculation could explain the variation observed at Yucca (shown in Figure 4b), special calculations can be performed for several events at Yucca and then compared with the predicted and the observed relative amplitudes. As of this writing, these calculations have not been performed.

Missing also is a convincing explanation for the low amplitude levels in west Pahute Mesa. However, one explanation might be that if a large high-Q plug beneath the Silent Canyon Caldera is centered on event GREELEY (E) (suggested by Spence (1973) and by the Caldera surface perimeter, taken from the map by Orkild et al. (1969) and drawn in Figure 1), then the larger first-motion values could be interpreted for STILTON (w) and for events in east

Der, Z. A., and T. McElfresh (1976). The effect of attenuation of the spectra of P waves from nuclear explosions in North America; SDAC-TR-76-7, Teledyne Geotech, Alexandria, Virginia. DDC: ADA 030857.

Johnson, M. S., and D. E. Hibbard (1957). Geology of the Atomic Energy Commission Nevada Proving Grounds Area, Nevada; U.S. Geological Survey Bulletin 1021-K, U.S. Government Printing Office, Washington, DC.

Fernald, A. T., G. S. Corchary, and W. P. Williams (1968). Surficial geologic map of Yucca Flats, Nye, and Lincoln counties; U.S. Geological Survey Map I-550.

Orkild, P. P., K. A. Sargent, and R. P. Snyder (1969). Geologic map of Pahute Mesa Nevada Test Site and vicinity, Nye County, Nevada; U.S. Geological Survey Map I-567.

Pahute as showing that they are not affected, on the path to RKON, by the effects of the high-Q plug. If, however, the high-Q plug is used to explain the low first-motion amplitudes, the effect must be due to ray refraction and divergence. We shall see that the variation is not as large at HNME, possibly because refractions at the edges of a high-Q plug do not seriously affect a more vertically departing ray.

Event TYBO (V) shows the largest deviation from the average M_s and m_b shown in Figure 4a. In a personal communication, L. Ramspott stated that TYBO had anomalously large amplitudes at Las Vegas and Mina , Nevada, to the east, and anomalously small amplitudes at 3 other Lawrence Livermore seismic stations at other azimuths. In Figure 4b, the contours which can be drawn for west Pahute Mesa suggest that if similar contours were drawn for any station of interest, an improved amplitude prediction could be made because the contours show TYBO to fit the overall pattern for west Pahute Mesa.

Note that because these contours cannot be drawn at HNME, this smooth, dramatic variation in contours is clearly a source-station effect for RKON, possibly due to the greater angle from the vertical for rays departing to RKON. This greater angle might enhance the refraction effects as the rays leave the high-Q plug.

Plots similar to those in Figures 4a,b have been created with M_s replaced with log(yield). Exactly similar conclusions may be reached, as would be expected from the exceedingly small M_s:yield scatter found by von Seggern (1976) for NTS events below the water table. The low variance of von Seggern's data can be represented by a plot of M_s:yield for the shots with declassified yields, given in Table I. These data are well represented by the equation $M_s = \log(\text{yield}) + 2.4$. (von Seggern set the absolute level of M_s, using a world-wide single-station network (WWSSN) of 10 stations for several large NTS shots.) The only noticeable change is that events above the water table move to the right in the m_b:log (yield) plot analogous to Figure 4a. This shift is expected because these events do not couple as well as events below the water table. Figure 1 indicates the distance (in meters) to the water table for events above the water table.

PILEDRIVER ()), a shot in granite, has a higher amplitude than west Pahute events possibly because of the source medium. Figure 4b shows that the location of PILEDRIVER also can be used to explain this observation.

Figure 5a is a plot of log(a) versus log(c) at RKON. The scatter shows substantial variation in wave shape. Variations appear during comparison of the waveforms for: SCOTCH (J), COMMODORE (I), REX (5), and TYBO (v) (Figure 5d). SCOTCH and REX are very similar in wave shape and, like TYBO, have a small first motion. The small first motion is typical of Pahute Mesa events. Yucca events, however, have a relatively large first motion that is indicated by the short-period vertical trace for COMMODORE.

Figures 5a,b show a substantial difference in the log(a) versus log(c) ratios between Pahute and Yucca. This effect could stem from multipathing or from the fact that, because the average velocity in the medium is lower at Yucca than at Pahute, the pP interference with the c amplitude is greater at Yucca, so that the first motion of the signal appears large in relation to the rest of the signal.

To test this hypothesis, the log(a) residual versus the theoretical 2-way travel time (2x depth/average velocity) is plotted (Figure 5c). The travel time has been normalized by the dominant period which the received P-wave signal would have if not affected by pP. (This dominant period, a function of yield, is determined later in this report.) The result shown in Figure 5c indicates a definite trend, that suggests that pP does have an effect. Whether the trend follows predicted detailed theory can only be determined by detailed calculations of complete theoretical waveforms, using techniques discussed by Blandford (1976).

One possible physical explanation for the behavior plotted in Figure 5c is that the a amplitude is actually unaffected by pP in any of the measurements. However, for very short, scaled delay times, the c phase is substantially reduced by the reflection of a. Thus, a has a positive residual with respect to the expected value for c. At slightly larger delays, the c phase is enhanced, while for even larger delays it is again reduced. The fact that the a minimum (c maximum) occurs at a time delay of approximately 0.5 times the dominant period is consistent with this interpretation.

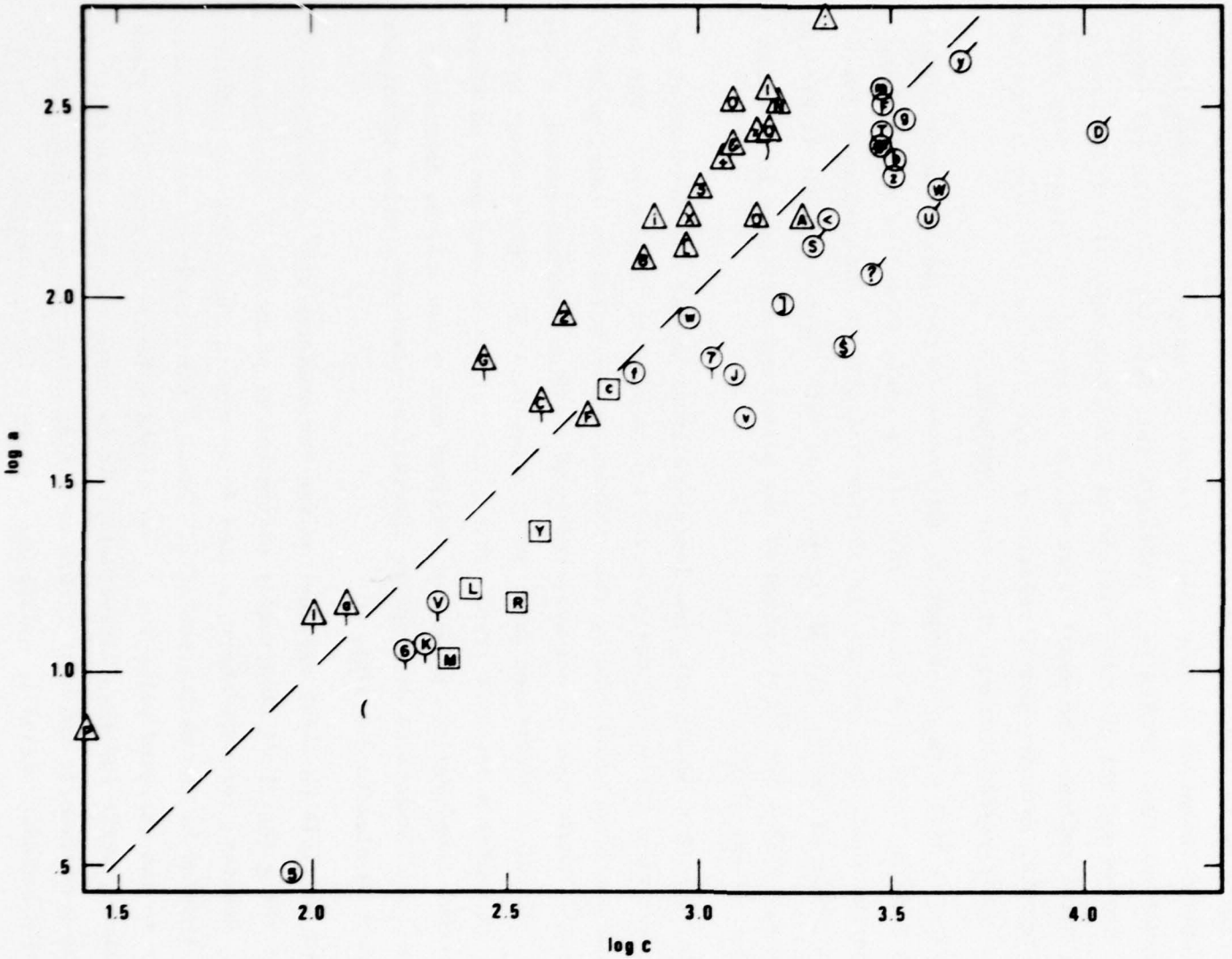

Figure 5a. RKON Station: Log (a) as a function of log (c). The dashed line is the least-squares line of slope 1.0 through all the data.

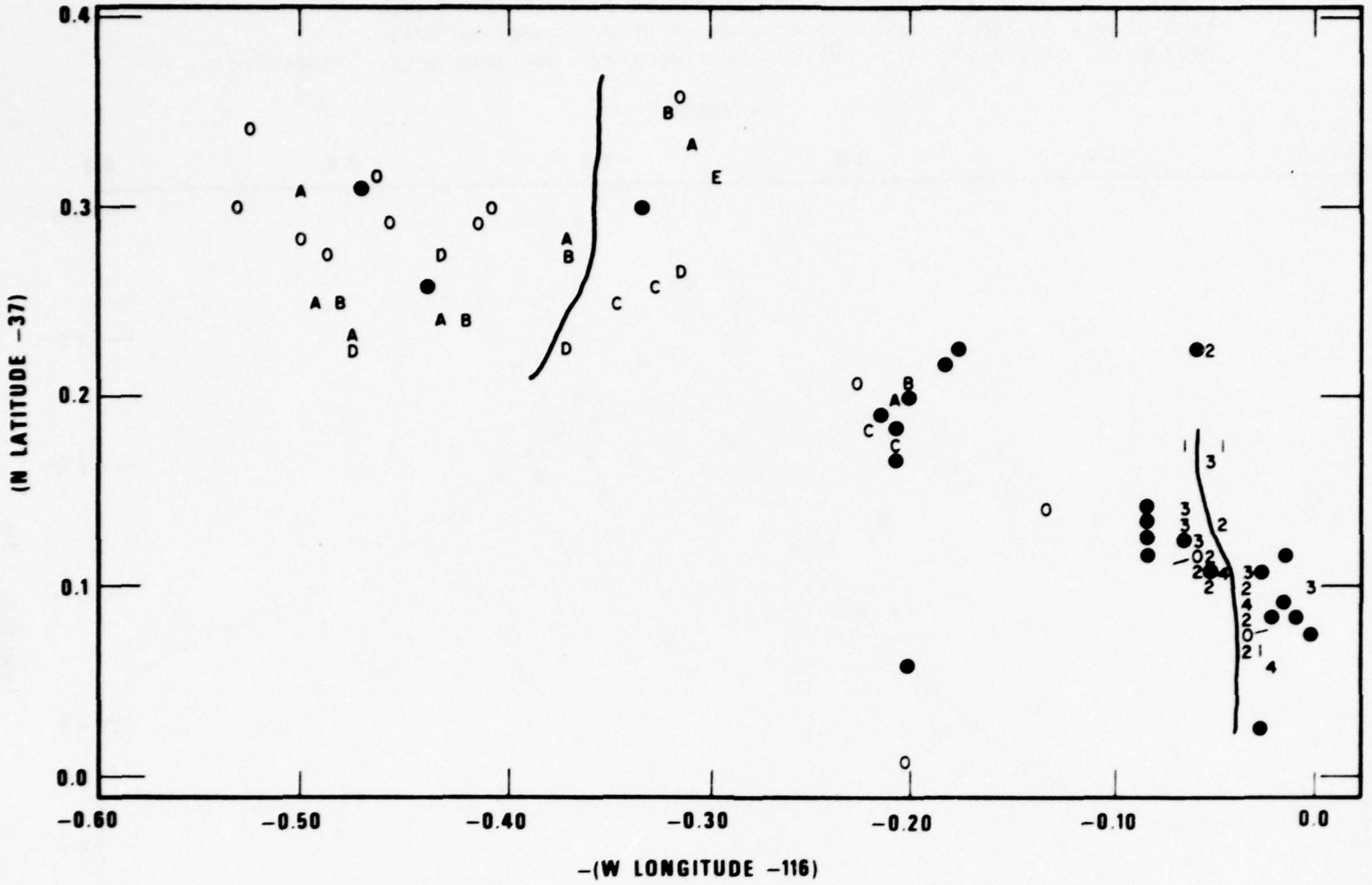

Figure 5b. RKON Station: Residuals of log (a) with respect to the dashed line in Figure 5a as a function of latitude and longitude at NTS. Events are identified in Table I and Figure 1.

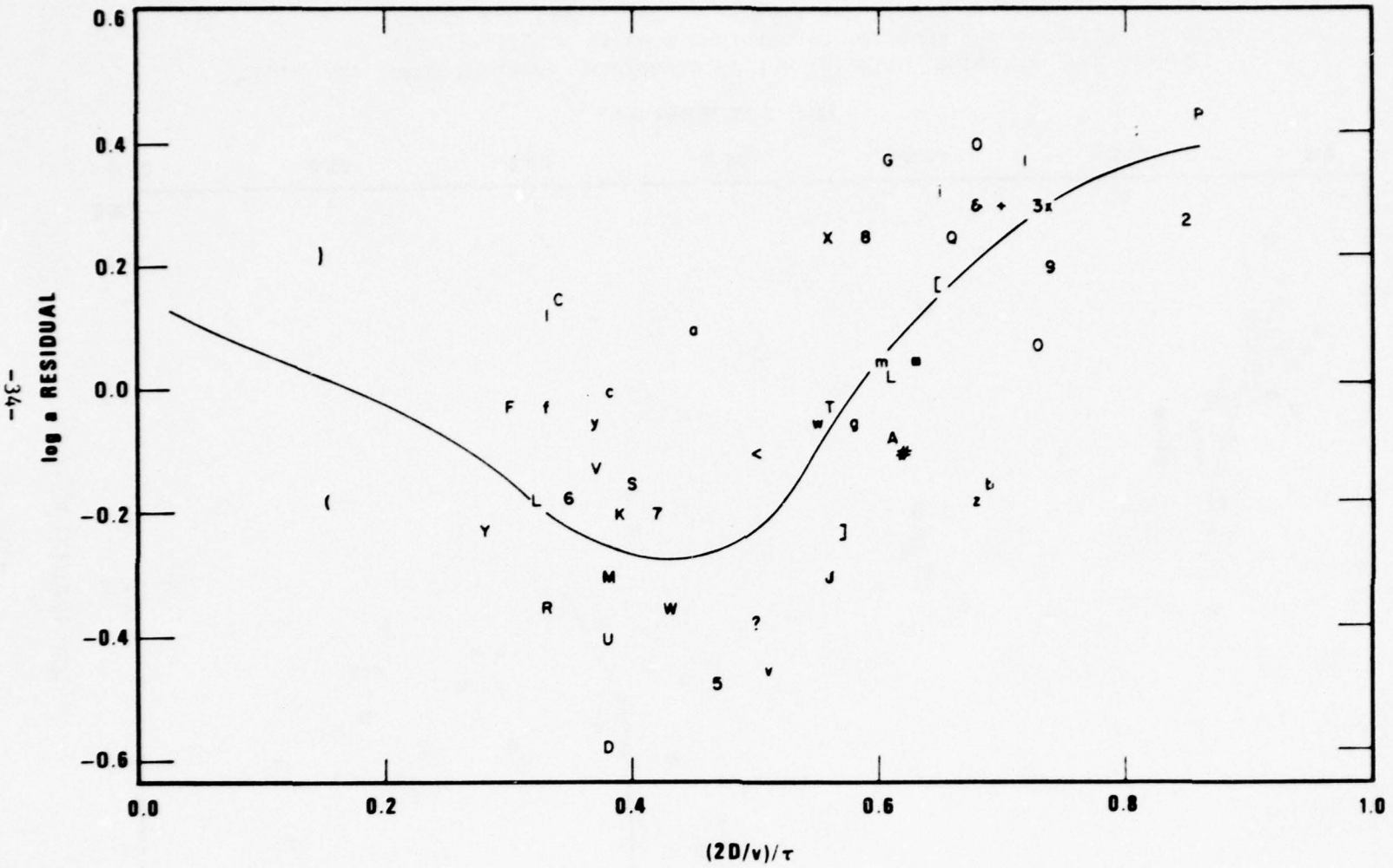

Figure 5c. RKON Station: Residuals of log (a) with respect to the dashed line in Figure 5a as a function of scaled 2-way pP travel time. The solid line is hand-drawn as a subjective estimate of the main data trends.

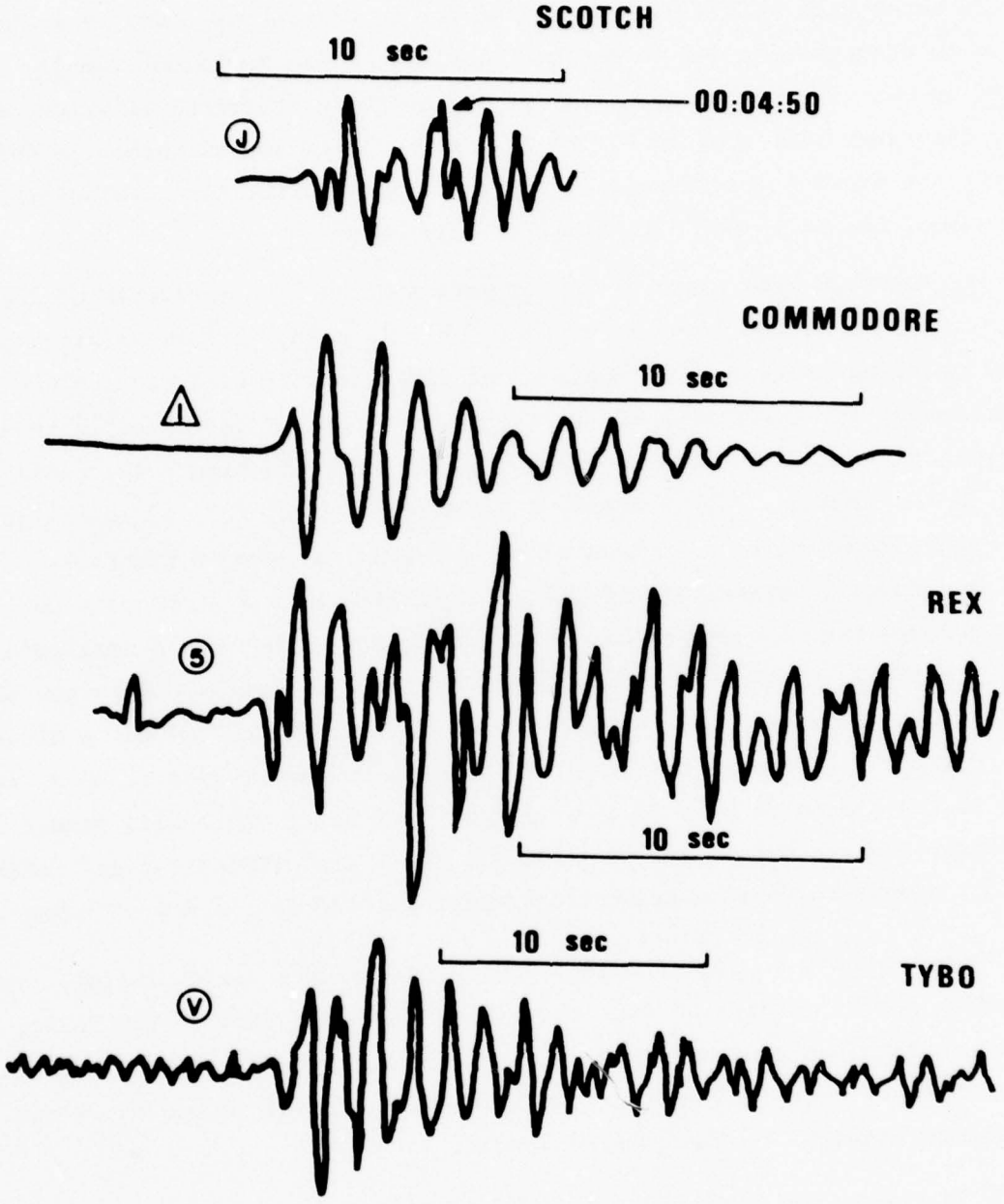

Figure 5d. RKON Station: Waveforms of the events SCOTCH, COMMODORE, REX, and TYBO to show the variety of possible signals.

The empirical results in Figure 5c suggest that the c amplitude, which in most cases will be the phase measured for magnitude, may vary by at least 0.6 units of magnitude due to depth of burial. While amplitude can increase by only 0.3 magnitude units, it may decrease, theoretically, to zero. Thus, the range indicated in Figure 5c does not seem implausible. In this report, the minimum delay occurred for shots in granite; for a velocity of 5.5 km/sec, the delay for PILEDRIVER is 0.17 sec.

Figures 6a,b show plots of log(c) versus M_s and the residuals of log(c) with respect to latitude and longitude. In this case, variations attributed to multipathing or to ray convergence and divergence in Figures 7a,b would be confounded by the variations due to the pP interference discussed in connection with Figures 5a,b. Thus, simple contours, like in Figure 4b, cannot be drawn in west Pahute. Curvature as a function of yield for the mean line for west Pahute seems more of a possibility in Figure 6a than in Figure 4a. Indications strongly suggest that if the waves of RKON have a short path (or no path) through the root of the Silent Canyon Caldera, then the c amplitude is substantially increased. However, this effect may be confounded by the magnitude-yield curvature. For example, though event STILTON (w) has a clear path from its position northwest of the caldera to the station at RKON, its yield is low enough to make its corner frequency high, which will result in a relatively large magnitude. Note in Figure 6b that SCOTCH (J) and CAMEMBERT (z) appear to be in a transition region between east and west Pahute.

Figure 7 shows a plot of log(c), corrected for pP, versus log(a). The correction factor is derived from the line through the data in Figure 5c, and is done to obtain a smoother m_b:M_s plot by removing the perturbing effects of pP. The result should be similar to Figure 4a -- log(a) versus M_s -- and this indeed seems to be the general result.

In Figure 8a the period of the c phase at RKON is plotted as a function of c versus M_s. The plot shows a strong trend over the depicted range of period (about 1.0 to 1.5 sec) and range of M_s (about 2.7 to 5.5) -- roughly equal to a yield ranging from less than 5 kt to slightly more than 1 megaton. This variation of period with M_s was used in Figure 5c to determine the dominant period with which to normalize the theoretical 2-way pP delay time. The same relationship will be used in similar plots, such as Figure 8c, below.

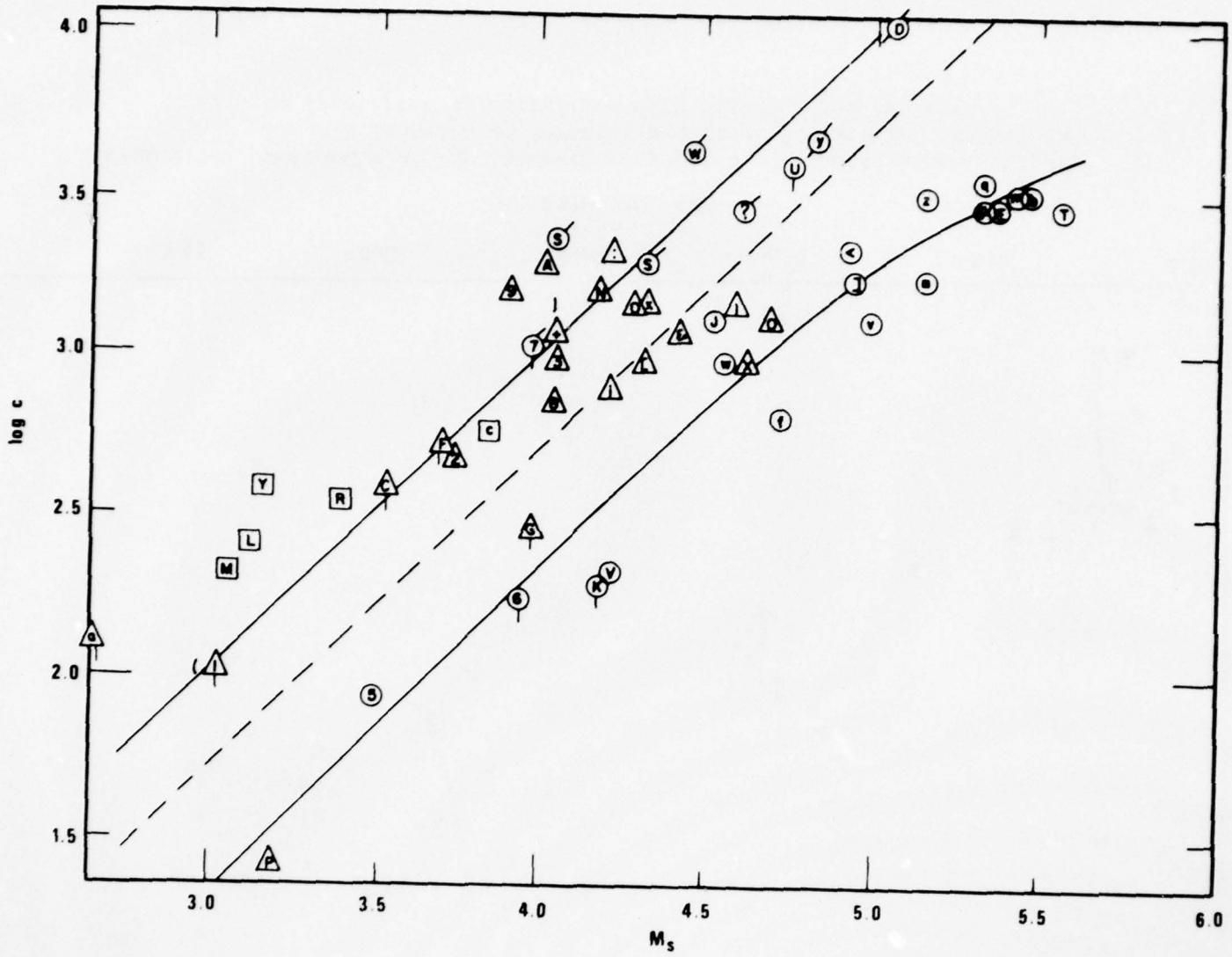

Figure 6a. c as a function of M_s at RKON. The dashed line is the least-squares lines of slope 1.0 through all the data. The solid curved lines are from Figure 3c with t* = 0.4 and with the vertical ordinate adjusted by eye separately to fit the West Pahute and all other data. Note that the East Pahute data also fit this latter curve (in contrast to the data in Figure 4a).

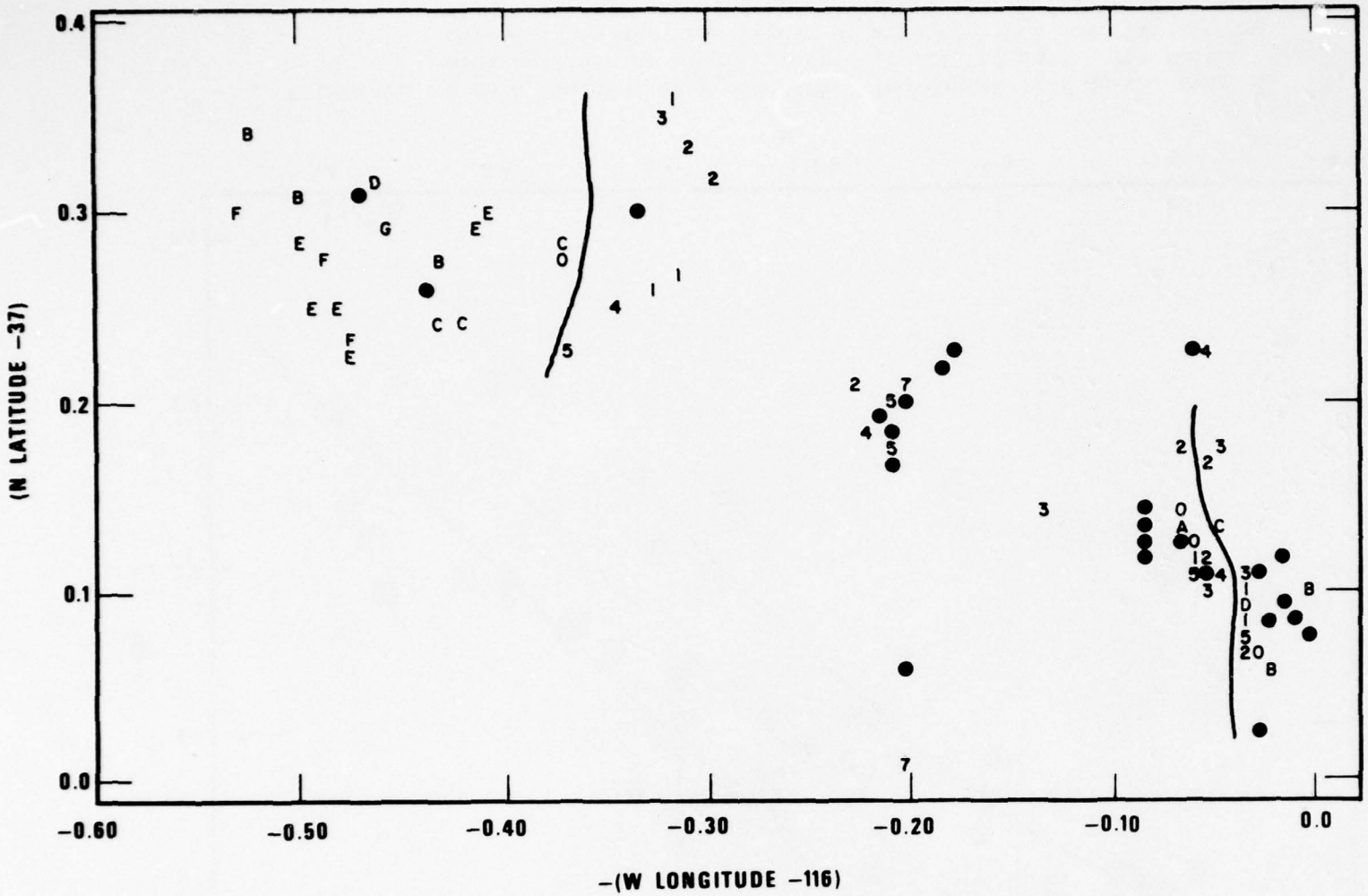

Figure 6b. Residuals of log (c) with respect to the dashed line in Figure 6a as a function of latitude and longitude at NTS. Events can be identified by comparison with Figure 1 and Table I.

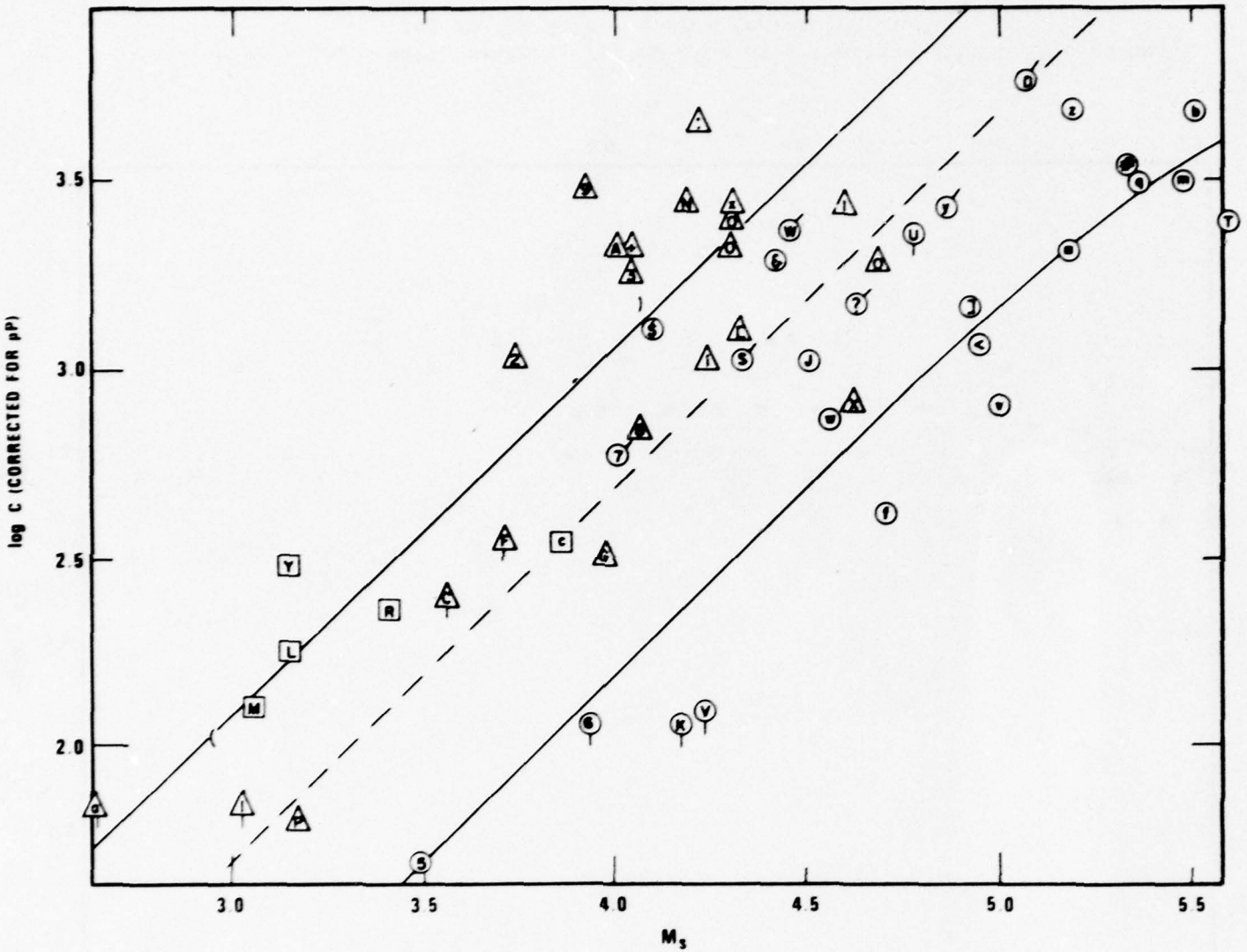

Figure 7. RKON Station: Log (c), with c corrected for pP, as a function of M_s. pP correction is given by the solid line in Figure 5c. The dashed line is the least-squares line of slope 1.0 through all the data. The solid curved lines are from Figure 3c with t* = 0.4 the with the vertical ordinate adjusted by eye separately to fit the West Pahute and all other data.

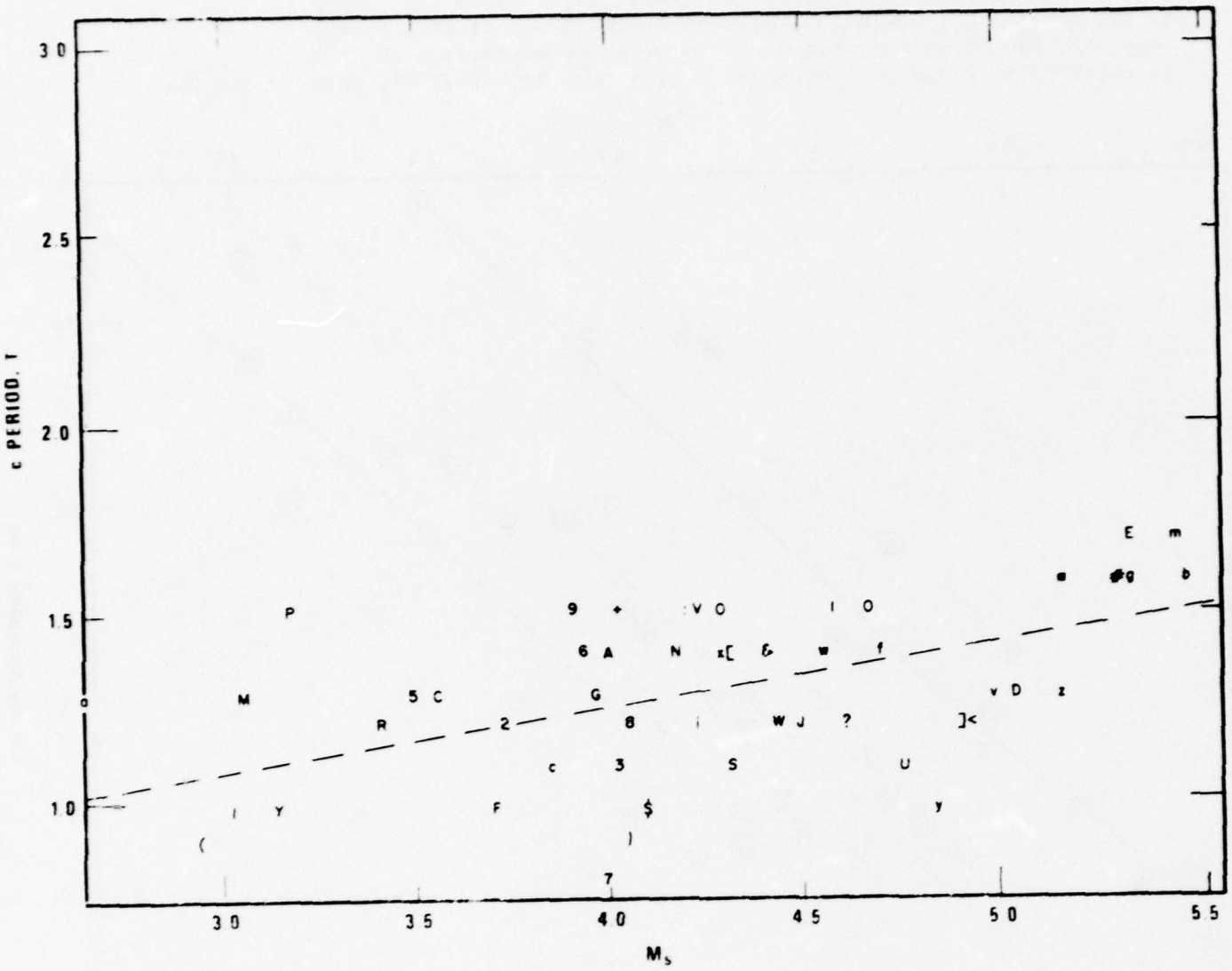

Figure 8a. RKON Station: Period of c as a function of M_s. The dashed line is the least-squares regression of M_s.

Note the large scatter about the mean line in Figure 8a, which the authors contend stems from geographic location and depth of burial (via the effect of pP interference). Figure 8b shows the residuals about the regression line plotted as a function of location; the contrast between east and west Pahute is apparent. Again, events SCOTCH (J) and CAMEMBERT (z) seem to be in a transition region. In Figure 8c these period residuals are plotted as a function of of normalized 2-way pP delay time, and a clear trend is evident. The events at either end of the trend are PILEDRIVER ()), and COBBLER (P). PILEDRIVER has an unusually short scaled delay time because of the high compression wave velocity in granite, and COBBLER has a longer than expected delay time because it was overburied for its yield and the medium had a low compression wave velocity. This graph suggests that the effects of pP alone may change the dominant period by as much as 0.7 sec. Note that this period correction will have an effect on m_b. At constant amplitude on a short-per-period LRSM system, this possible ±0.35-sec variation in period around 1.2 sec. corresponds to a range of 0.34 magnitude units in the factor 1/GT. In summary, Figure 8a shows the effect of yield on the dominant period. Figure 8b shows the effect of geographic location, and Figure 8c shows the effect of pP. While all effects are significant, note that they are linked; for example, large events are deep and in Pahute Mesa. Only calculations of each event can disentangle these effects.

Most of the trend toward short periods, shown in Figure 8c, can be traced to the 2 granite shots. Although the periods may be short because of the unique material properties of granite, that argument is weak because the granite RDP source seems to be adequate to explain the teleseismic magnitude versus yield curves for well-contained explosions in all source regions at NTS. Thus, there is no clear reason to omit the data from the shots truly set off in granite.

In Figures 9a, b, are plots similar to those in Figures 6a,b. The difference is that in Figures 9a,b the c amplitude has been corrected for system response at its observed period, and the resulting amplitude, divided by T, has been plotted. Considering the variety of influences on observed period already discussed, probably no correction for period would have any substan-

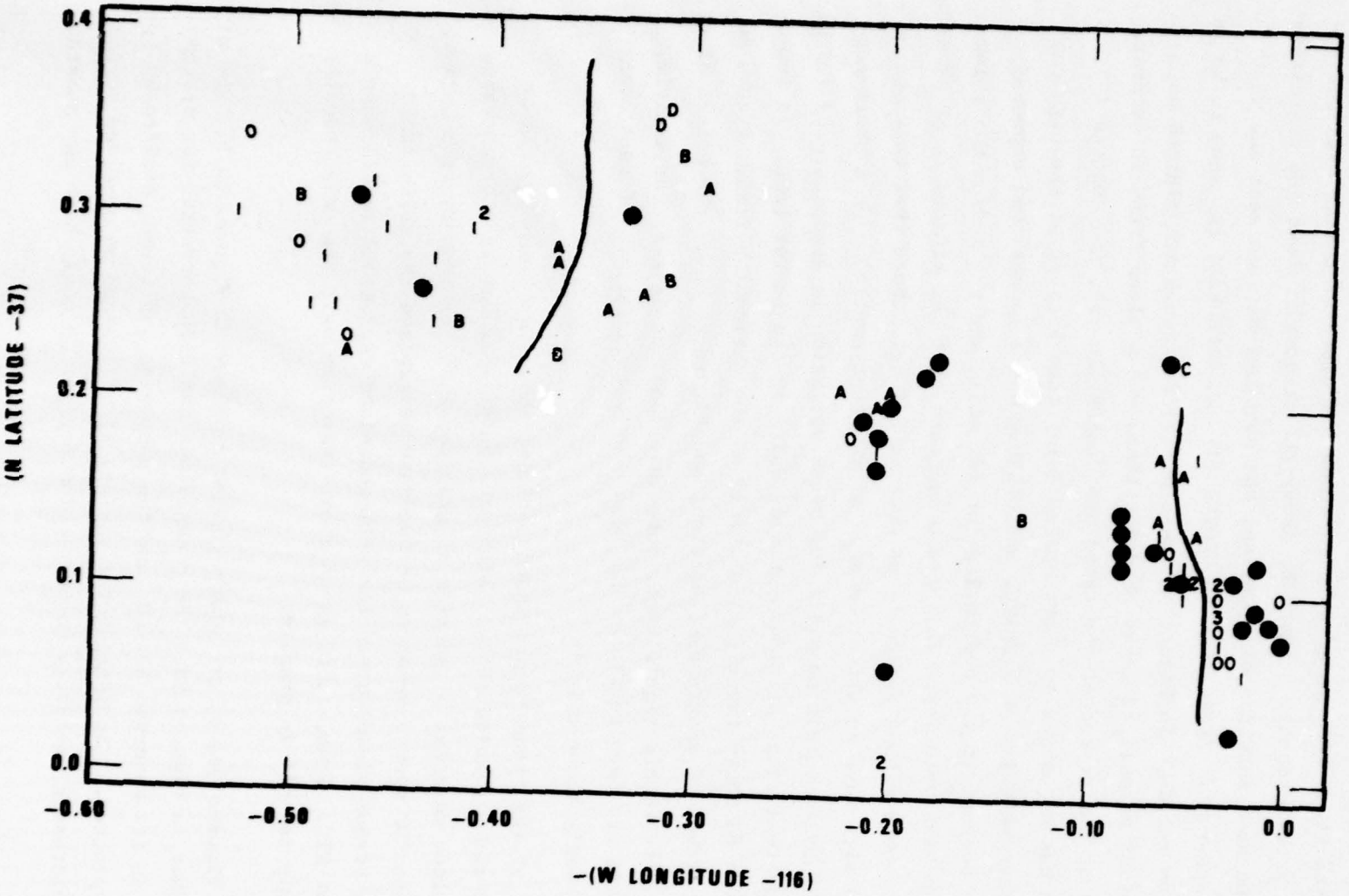

Figure 8b. RKON Station: Residuals, in tenths of a seconds, of the c period with respect to the dashed line in Figure 8a as a function of latitude and longitude at NTS. "A" corresponds to 0.1 to 0.2 sec below the line; "1" corresponds to 0.1 to 0.2 sec above the line. Events are identified in Table I and Figure 1.

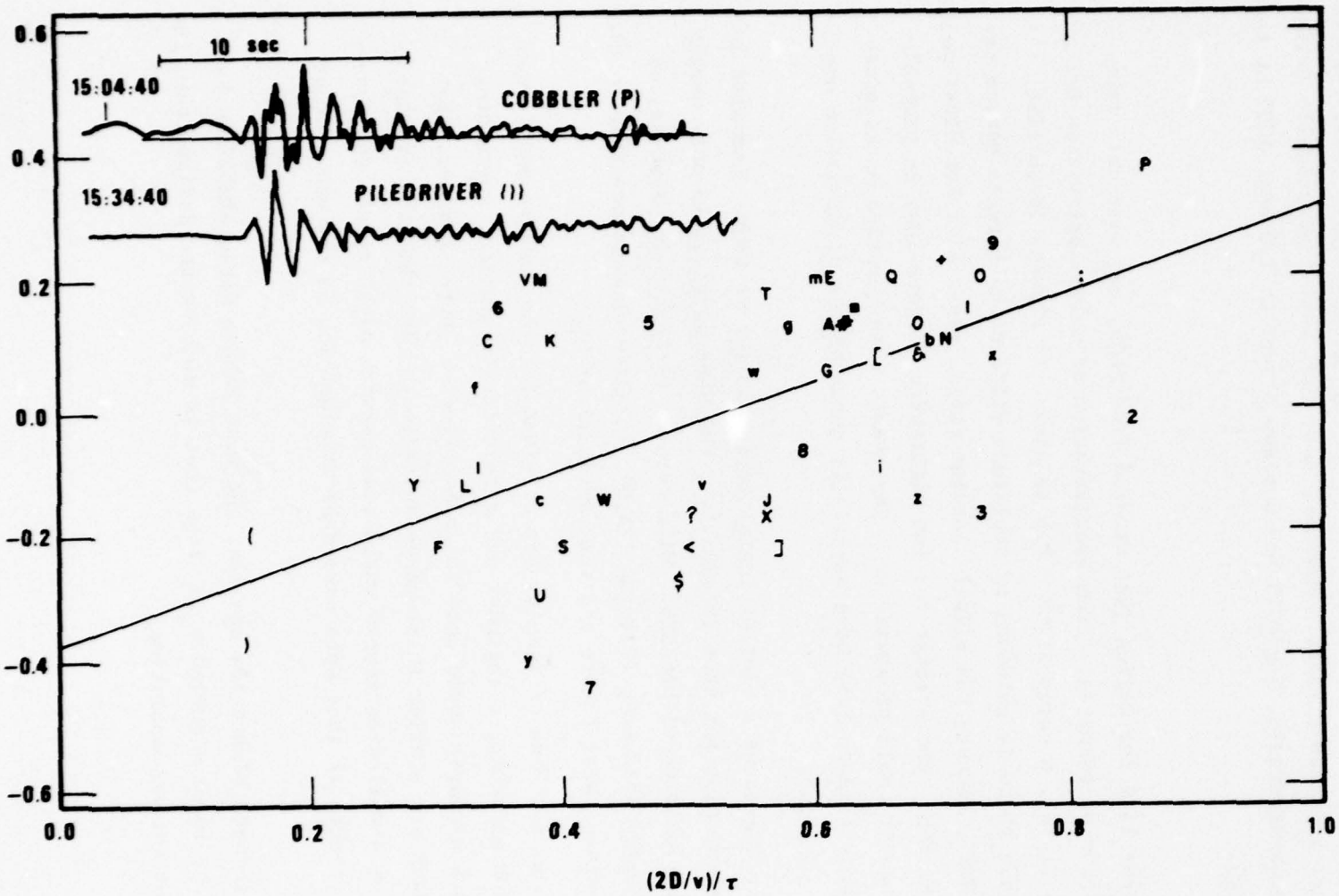

Figure 8c. RKON Station: Residuals, in tenths of a second, of the c period with respect to the dashed line in Figure 8a as a function of scaled 2-way pP travel time. The solid line has been subjectively drawn to point out the trend in the data. The RKON waveforms for 2 events at either end of the trend, PILEDRIVER ()) and COBBLER (P) are included in the upper left-hand corner.

tial clear-cut effect on the scatter of the m_b:M_s diagram; in fact, Figures 6 and 9 are remarkably alike. However, note that both theoretically (without pP) and experimentally, log(c/T) has a slope closer to 1.0 near 1000 kt than does log(c).

HNME

Figures like the series just studied from RKON, but with data from HNME will now be examined. From consideration of values derived in Der and McElfresh (1976), a value of t* = 0.6 is used. In Figures 10a,b like Figures 4a.b there is evidence of amplitude differences between source regions at NTS. Because the signal-to-noise ratio, especially for first motion, is lower at HNME, the scatter for low magnitudes (Figure 10a) is probably greater than it would otherwise be. The events with question marks after their symbols (Figure 10b) have especially questionable first-motion amplitudes due to noise.

Figure 11a shows a plot of log(a) versus log(c) at HNME. Compared to the equivalent plot for RKON (Figure 5a), the HNME waveform is only weakly affected by location within NTS. With respect to amplitude, however, by plotting log(c) versus M_s (Figures 12a,b), it again appears possible to distinguish between west Pahute and the remainder of NTS.

The same patterns of results are obtained for the c-phase amplitudes at both RKON and HNME, a regional and a teleseismic station, suggesting that network averages would show the same effects. Note, however, that RKON and HNME are similar in distance and azimuth, and that the average results from a well-distributed world-wide network might reduce the above-mentioned effects if they were caused by multipathing in the upper crust structure.

Note in both Figure 10a and 12a, the west Pahute data, signified by open circles, forms a curved m_b:M_s line that is much better defined than the line for the entire population.

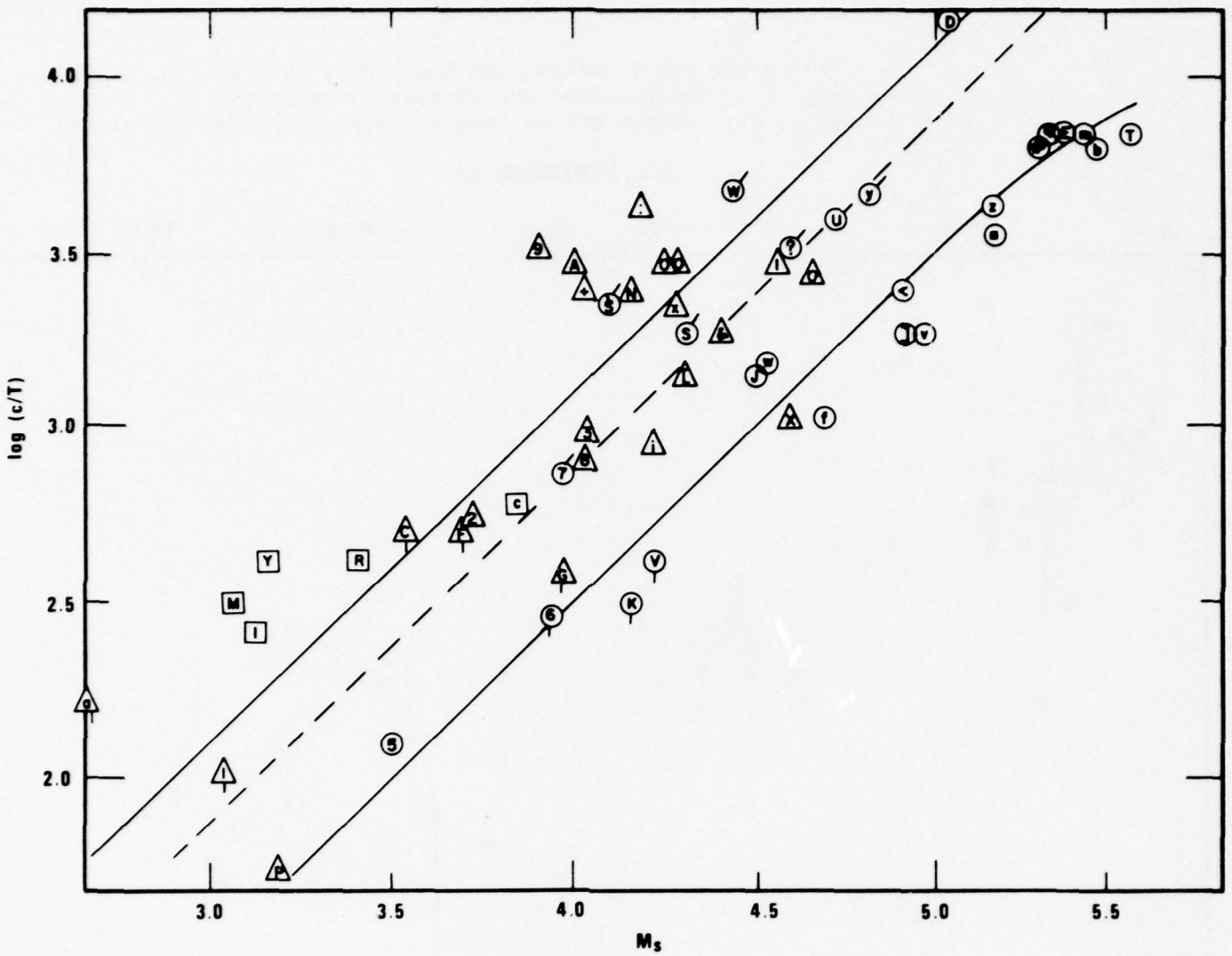

Figure 9a. c/T with c corrected for instrument response at period T as a function of M_s at RKON. The dashed line is the least-squares line of slope 1.0 through all the data. The solid curved lines are from Figure 3e with t* = 0.4 and with the vertical ordinate adjusted by eye separately to fit the west Pahute and all other data.

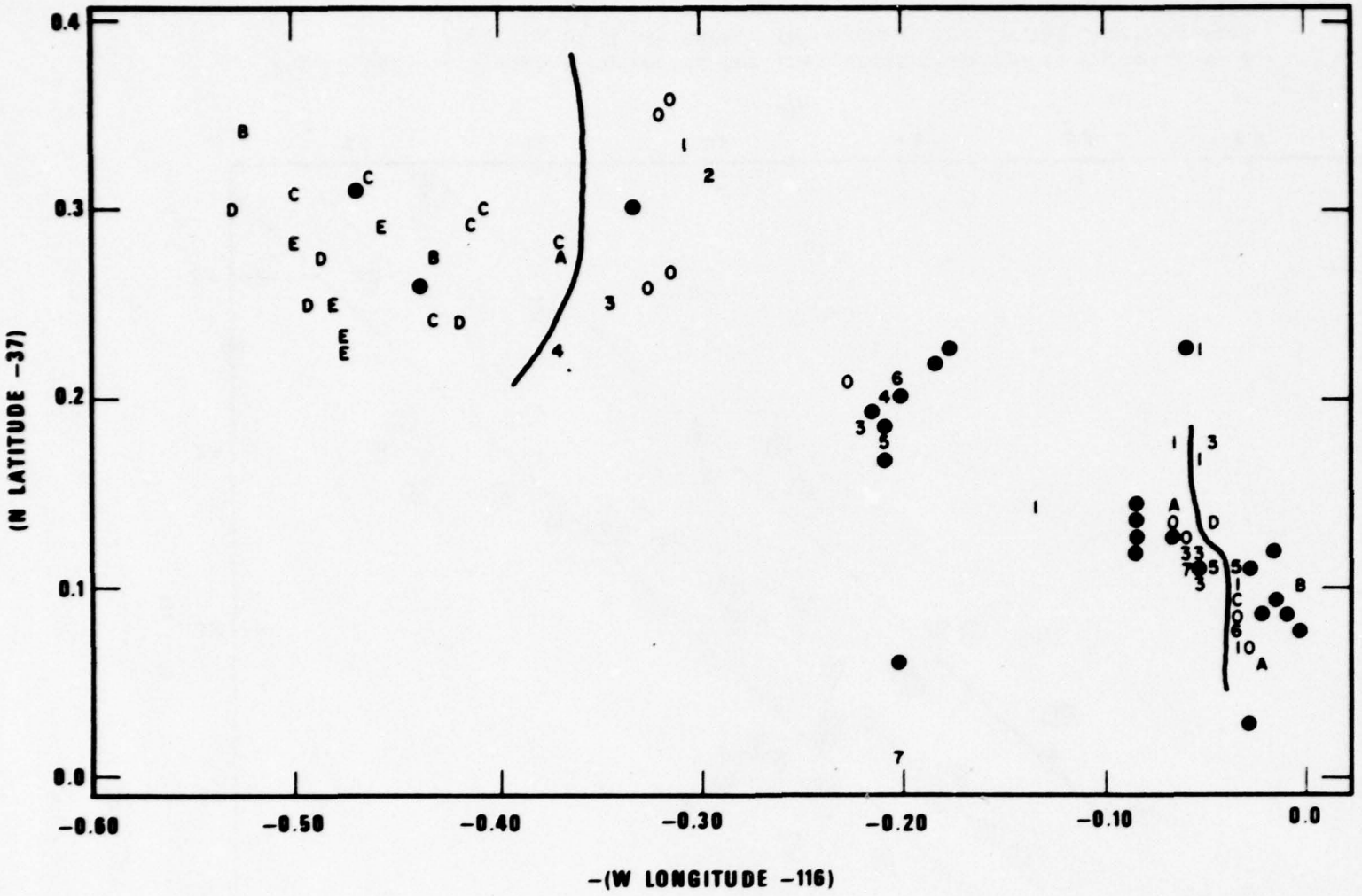

Figure 9b. Residuals with respect to the dashed line in Figure 9a as a function of latitude and longitude at NTS. Events may be identified by comparison with Figure 1 and Table I.

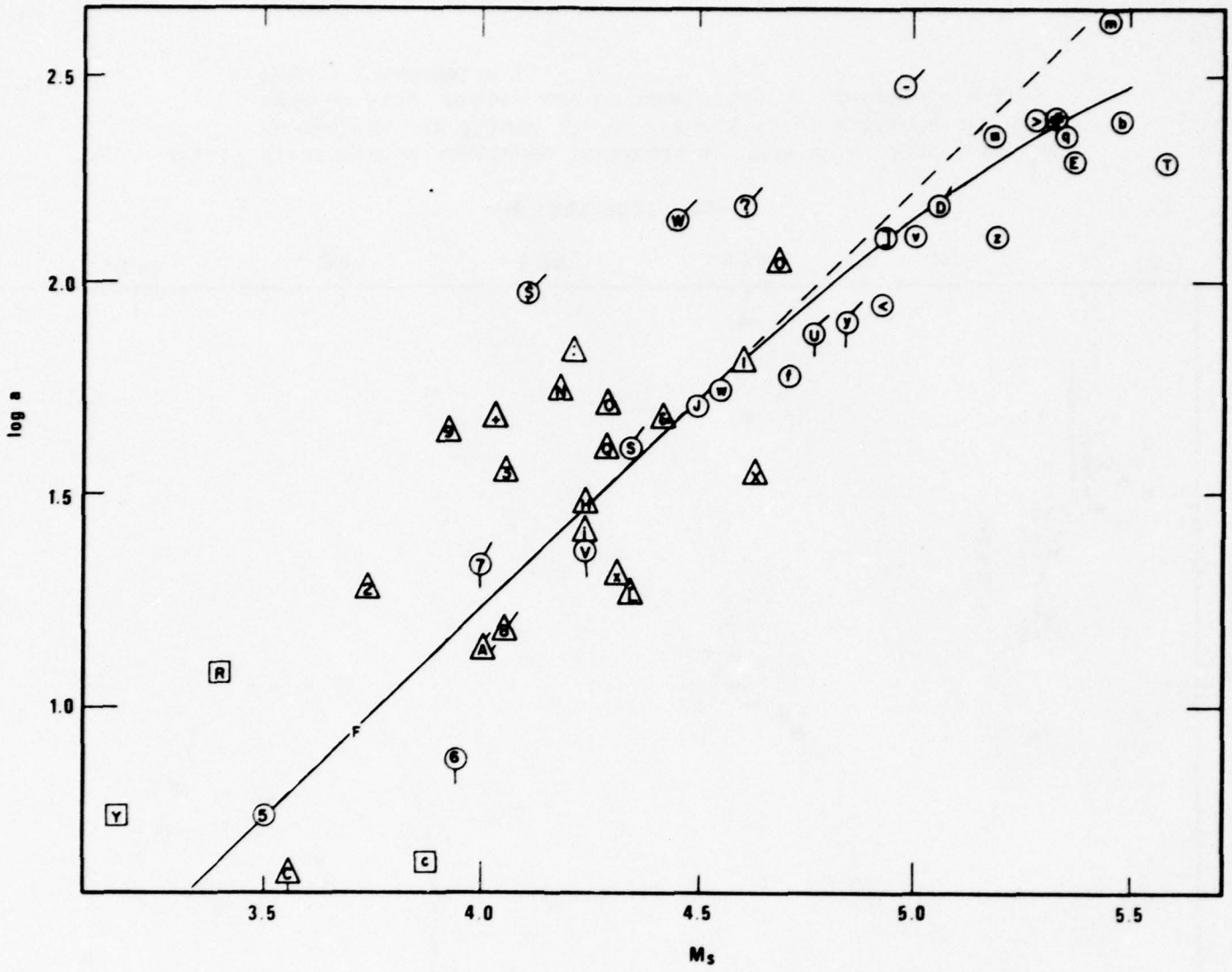

Figure 10a. $\underline{a}$ as a function of M_s at HNME. The dashed line is the least-squares line of slope 1.0 through all the data. The solid curved line is from Figure 3a with t* = 0.6 and with the vertical ordinate adjusted by eye to fit the data.

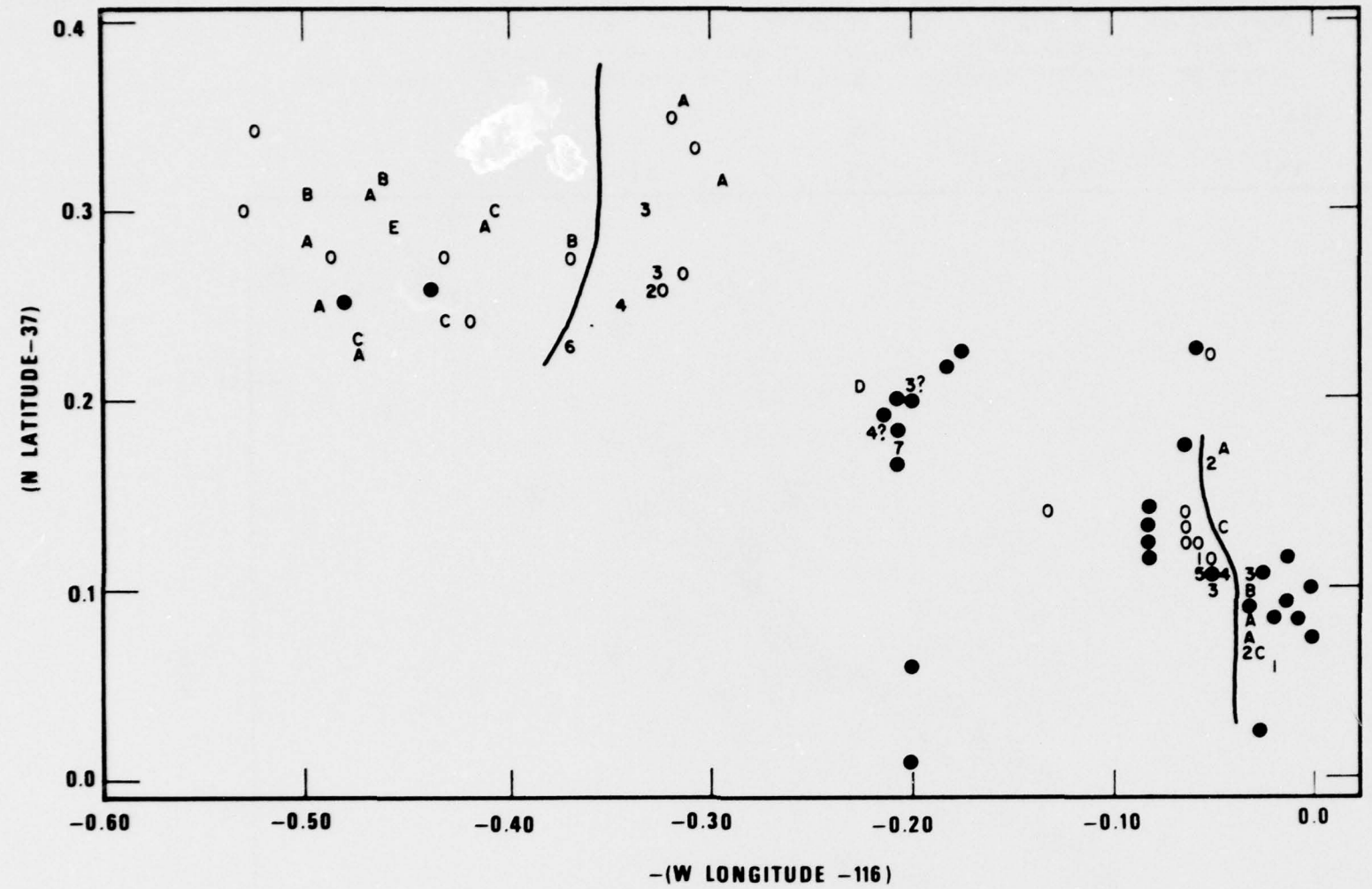

Figure 10b. First-motion amplitude residuals at HNME with respect to the dashed line in Figure 10a as a function of latitude and longitude at NTS. Events may be identified by comparison with Figure 1 and Table I.

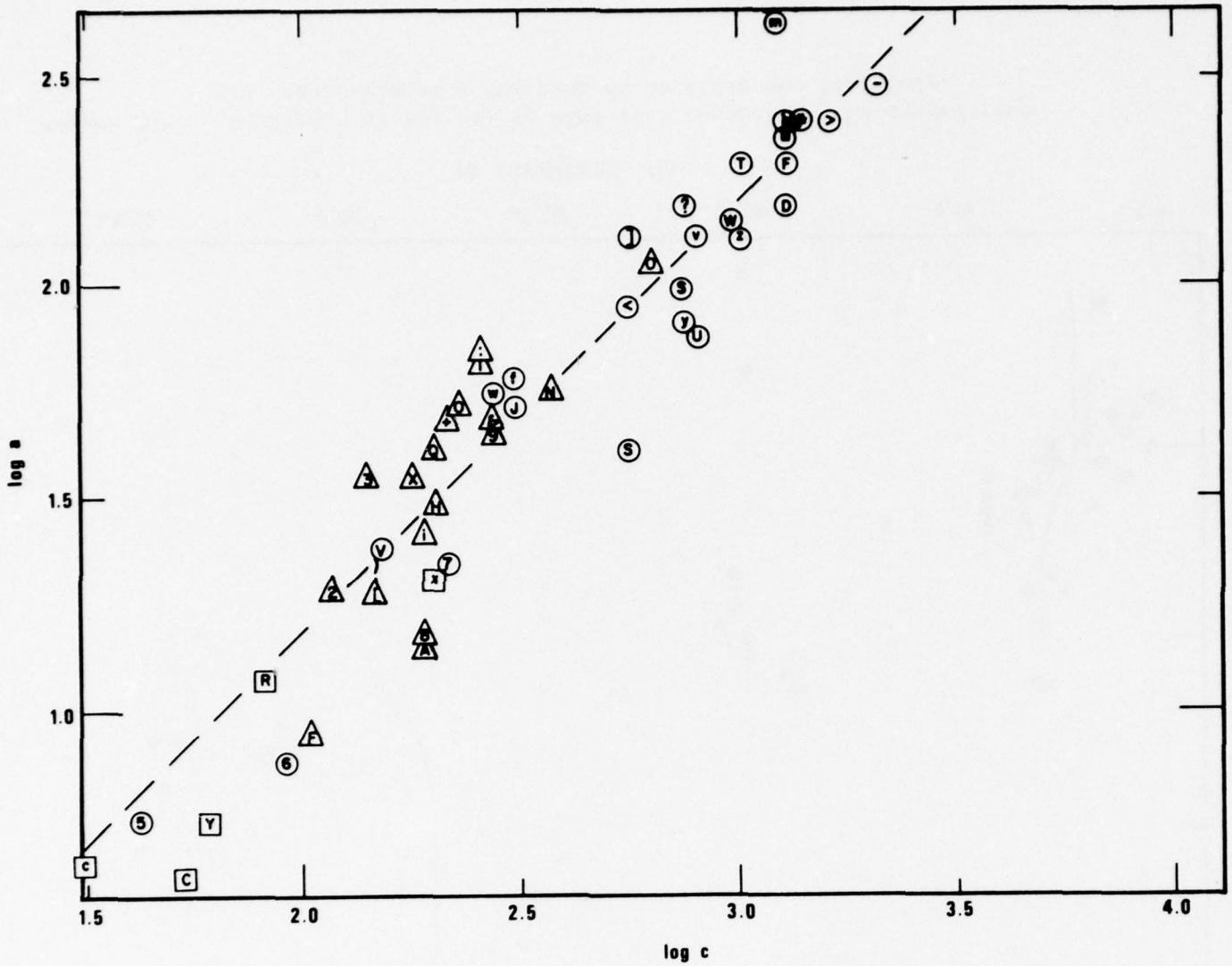

Figure 11a. a as a function of c at HNME. The dashed line is the least-squares line of slope 1.0 through all the data.

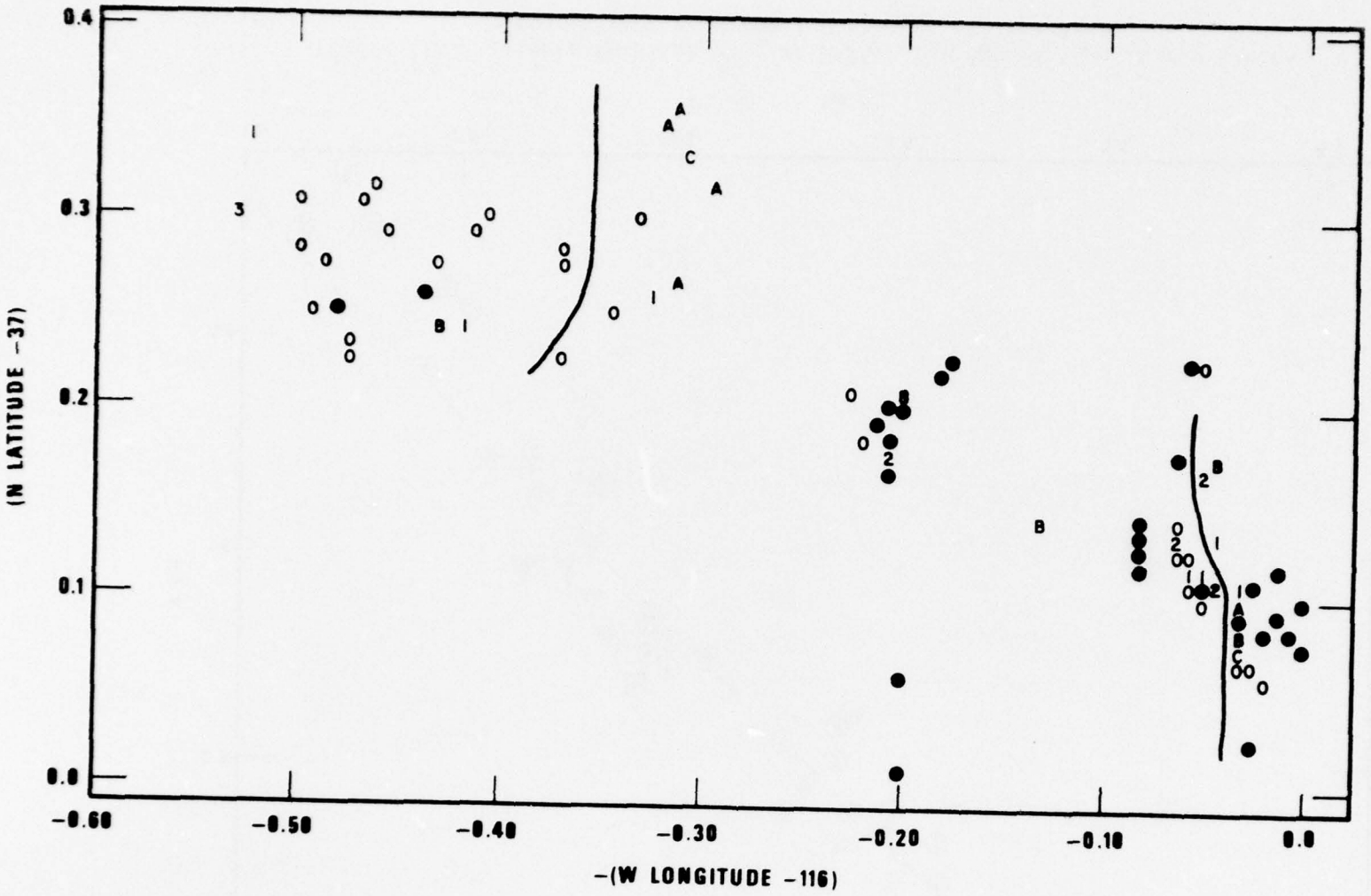

Figure 11b. Residuals of log (a) at HNME with respect to the dashed line in Figure 11a as a function of latitude and longitude.

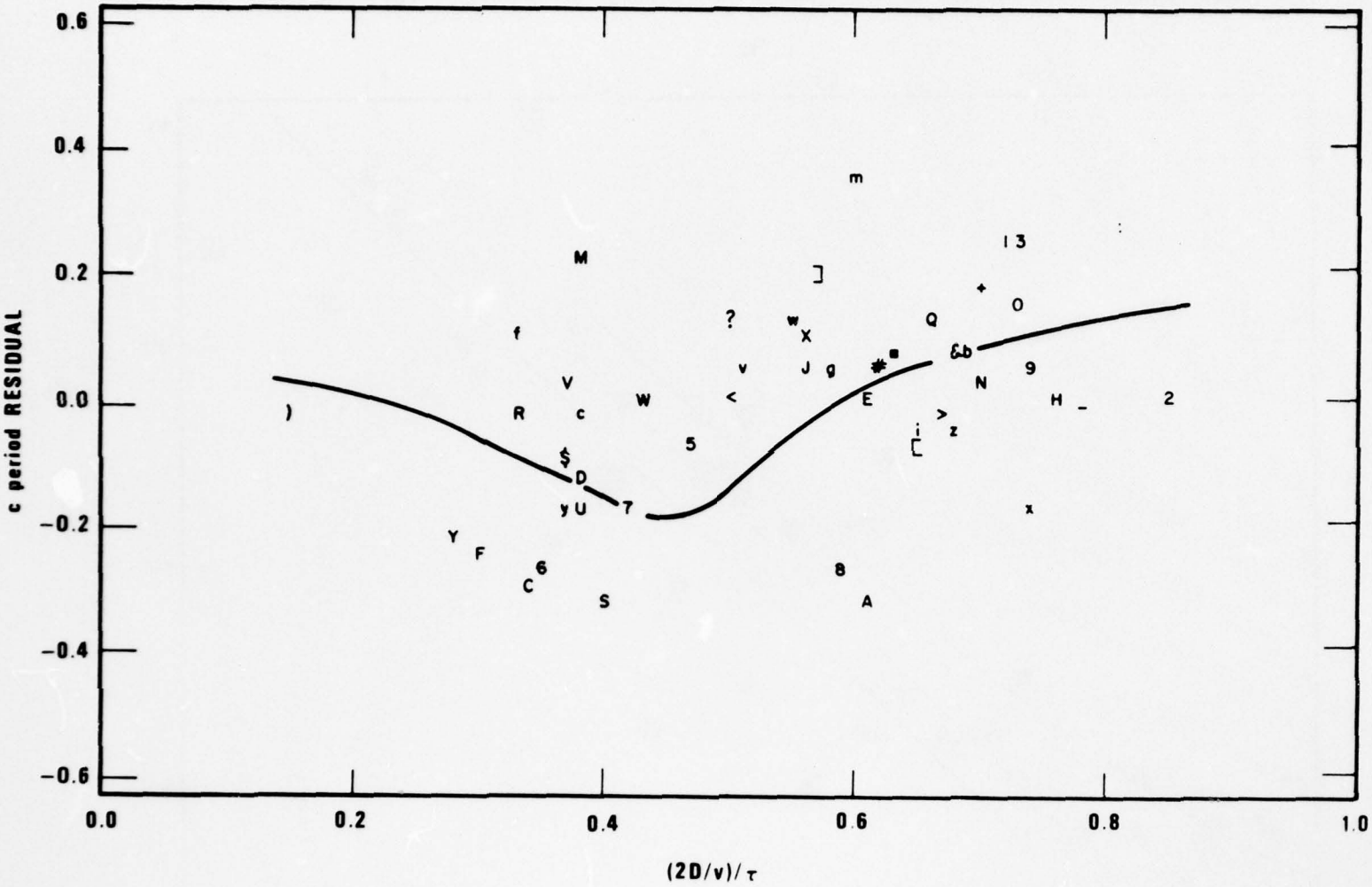

Figure 11c. Residuals of log (a) at HNME with respect to the dashed line in Figure 11a as a function of scaled 2-way pP travel time. The solid line is hand-drawn as a subjective estimate of the mean data trends.

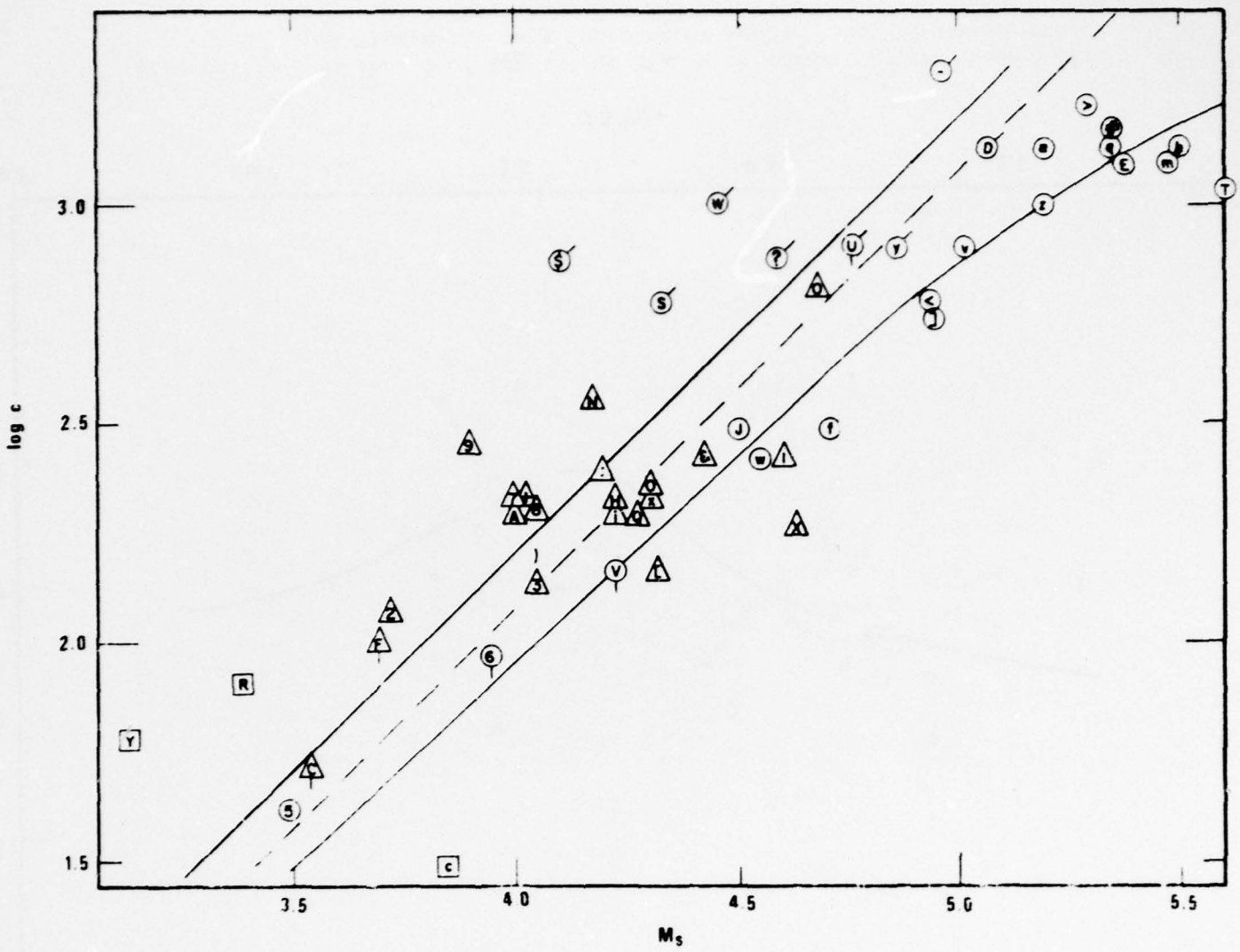

Figure 12a. c as a function of M_S at HNME. The dashed line is the least-squares line of slope 1.0 through all the data. The solid curved lines are from Figure 3c with t* = 0.6 and with the vertical ordinate adjusted separately by eye to fit the West Pahute and all other data.

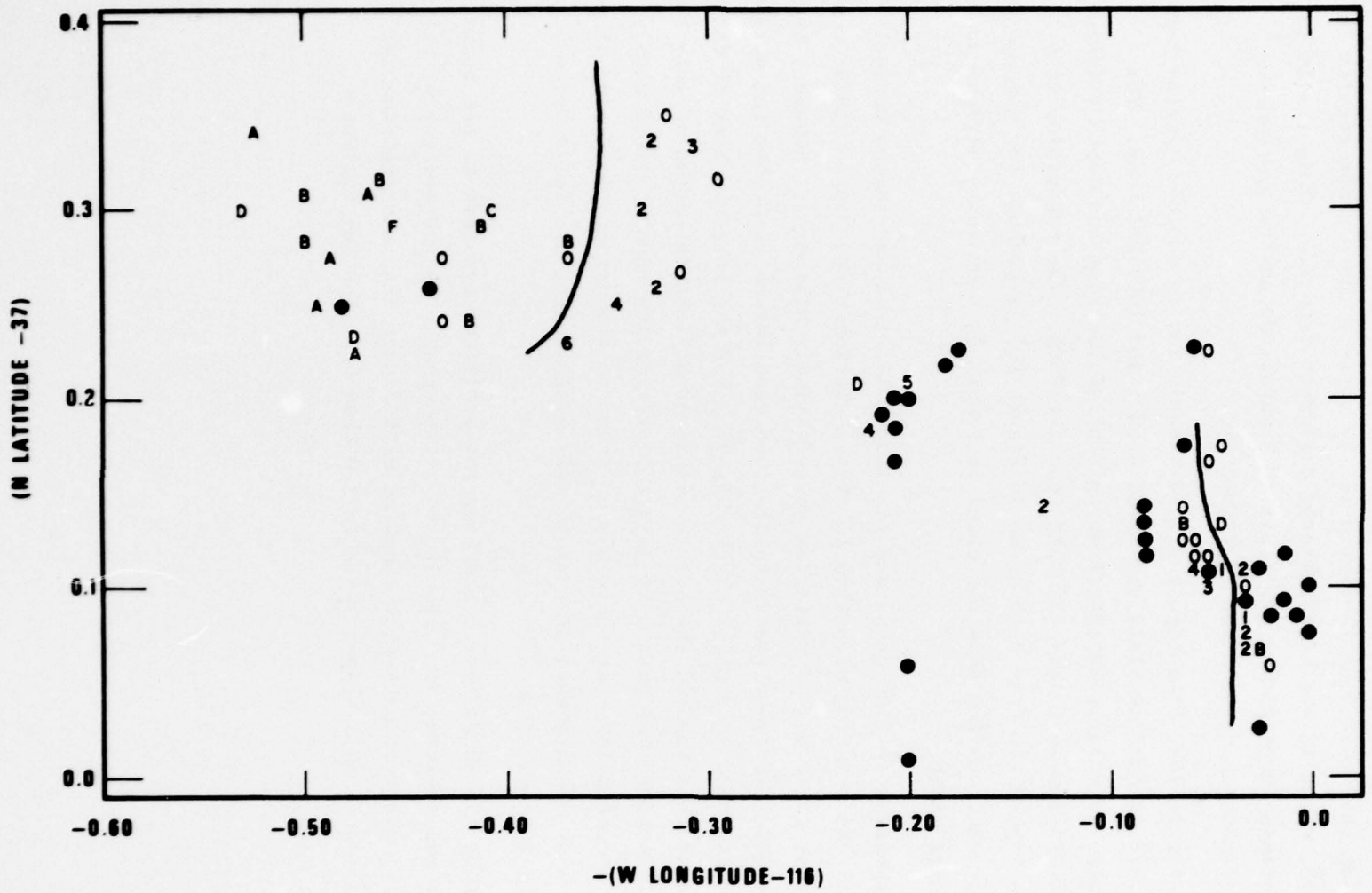

Figure 12b. c residuals with respect to the dashed line in Figure 12a at HNME as a function of latitude and longitude at NTS. Events may be identified by comparison with Figure 1 and Table I.

Using the solid line in Figure 11c to correct the $\underline{c}$ phase results in Figure 13, which is not significantly different from 12a. This result is not surprising considering the small (0.3 magnitude units) maximum-to-minimum excursion curve drawn in Figure 11c.

In Figure 14a, like Figure 8a, is a variation in dominant period between 1.0 and 1.6 seconds as yield varies between 5 and 1000 kilotons. The percentage variation resulting from epicentral location and depth (Figures 14b,c) seems somewhat less for HNME than for RKON. The regression line drawn in Figure 14c (the same drawn in Figure 8c) is perhaps too steep. On the other hand, unlike RKON the trend in Figure 8c does not seem dependent on the granite point.

Inspection of Figures 8a and 14a leaves little doubt that a variation exists in the relation of period to yield. Springer and Hannon (1973) concluded that there was no variation at teleseismic distances. However, they had available far fewer events to plot and were forced to accept the period measurements made in routine shot analyses. For the larger amount of data analyzed in this report, the scatter is so great that selection of only 10 points (the number of data available to Springer and Hannon) could easily lead to a conclusion that there was no trend to the data. Also, many of the routine shot measurements are undoubtedly contaminated by "false cycles", as discussed in connection with Figure 2.

Figure 15a shows that correcting for amplitude response at the measured period T and dividing by T results in little change in the scatter of the m_b: M_s curve. However, note that compared with Figure 12a, the experimental log ($\underline{c}$/T) curve as a slope closer to 1.0 than does the log ($\underline{c}$) curve.

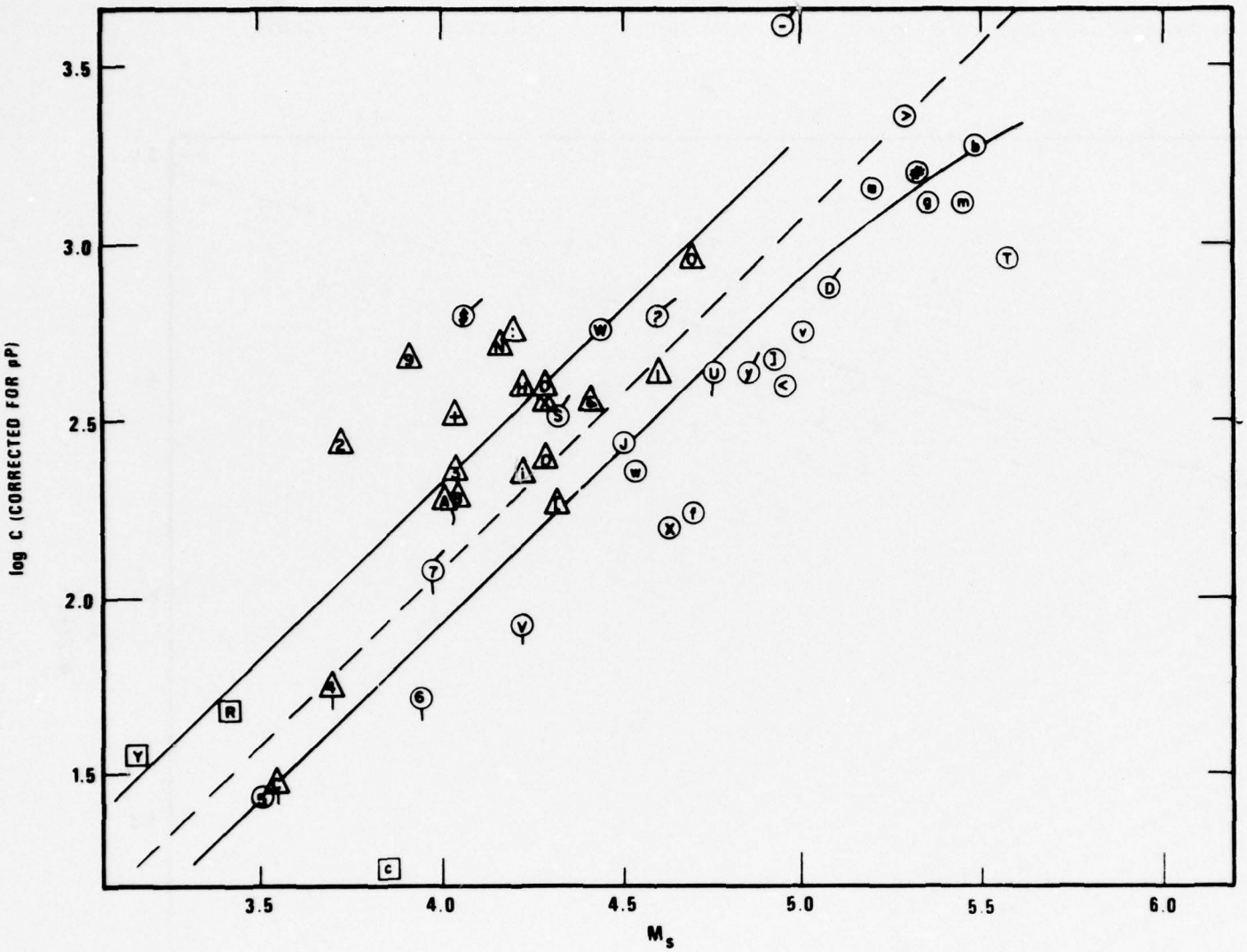

Figure 13. c plus pP correction for c at HNME as a function of M_s. pP correction given by the solid line seen in Figure 11c. The dashed line is the least-squares line of slope 1.0 through all the data. The solid curved lines are from Figure 3a with t* = 0.6 and with the vertical ordinate adjusted separately by eye to fit the west Pahute and all other data.

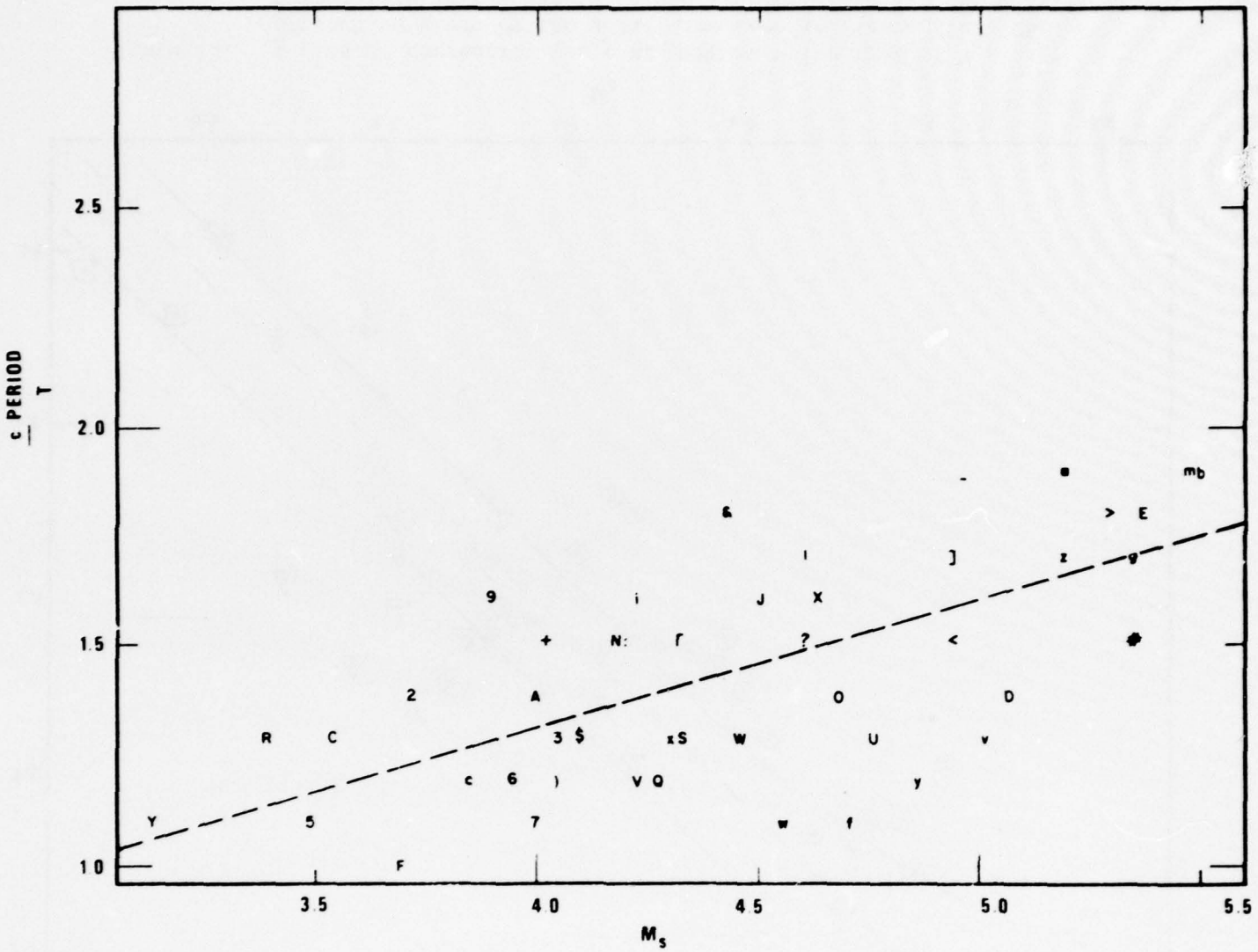

Figure 14a. Period of c at HNME as a function of M_s. The dashed line is the least-squares regression on M_s.

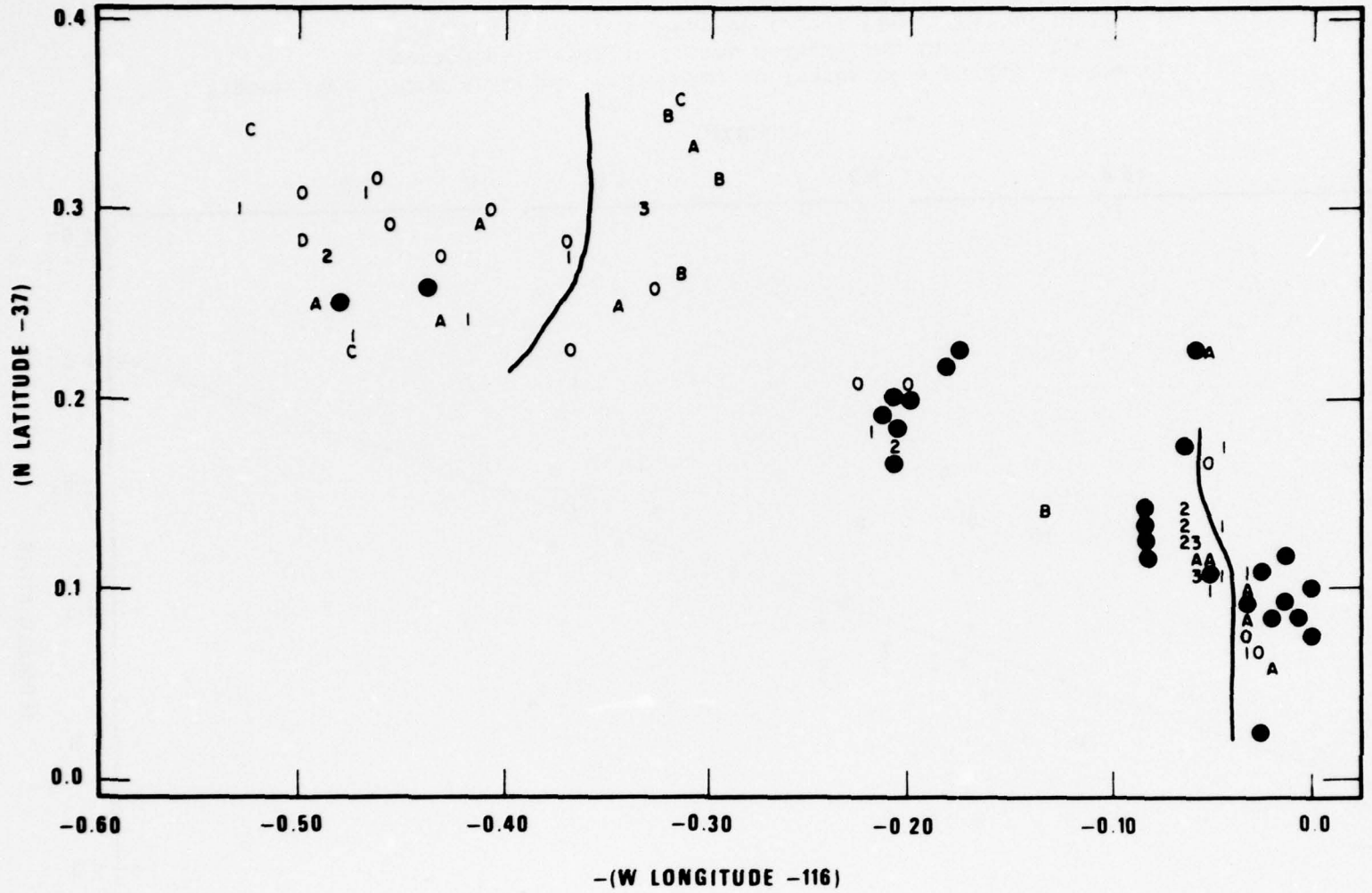

Figure 14b. Residuals of the c period at HNME in tenths of a second with respect to the dashed line in Figure 14a as a function of latitude and longitude. "A" corresponds to 0.1-0.2 seconds above the line. Events may be identified by comparison with Figure 1 and Table I.

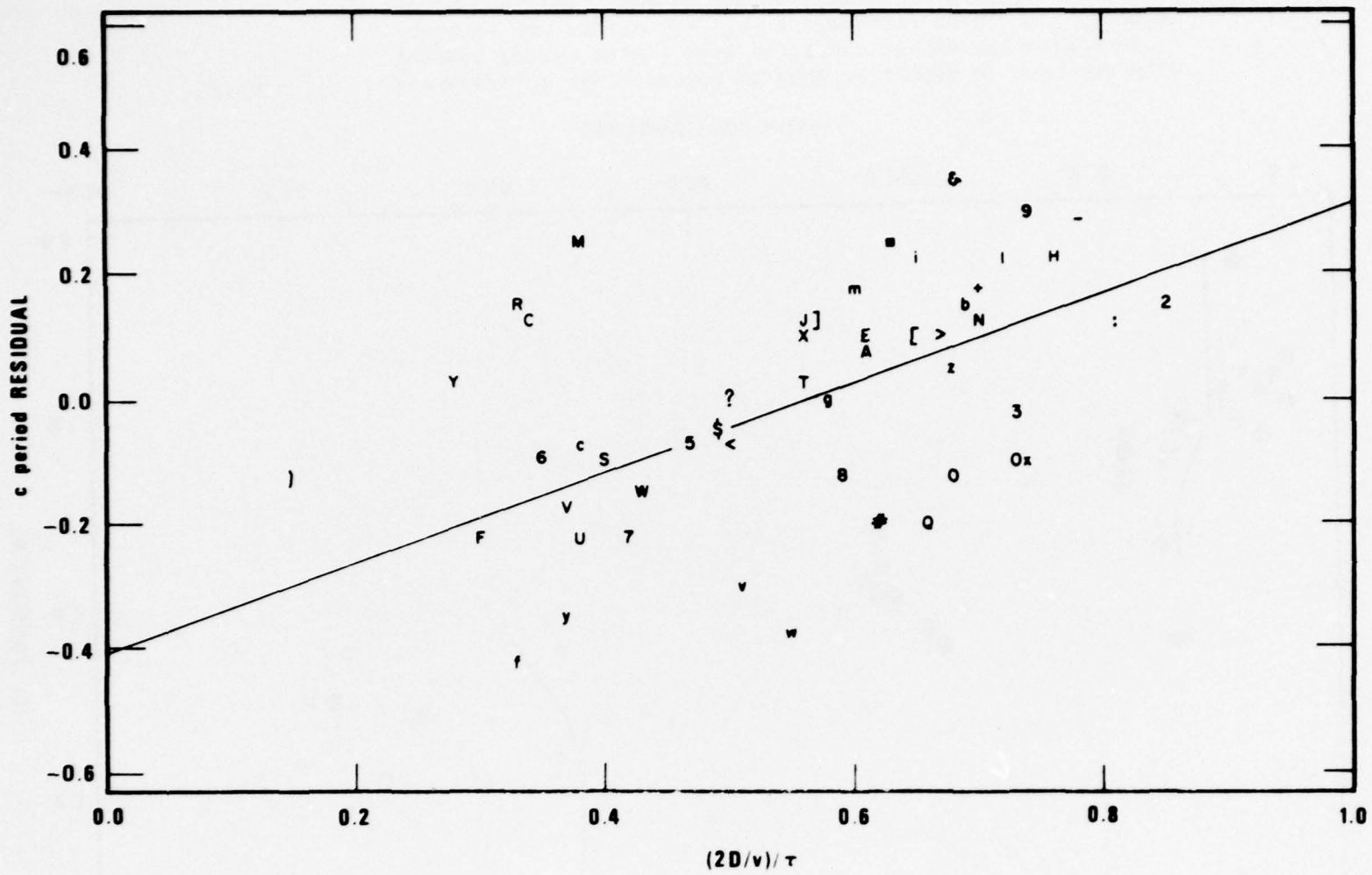

Figure 14c. HNME Station: Residuals, in tenths of a second, of the c period with respect to the dashed line in Figure 14a as a function of scaled 2-way pP travel time. The solid line is hand-drawn as a subjective estimate of the main data trends.

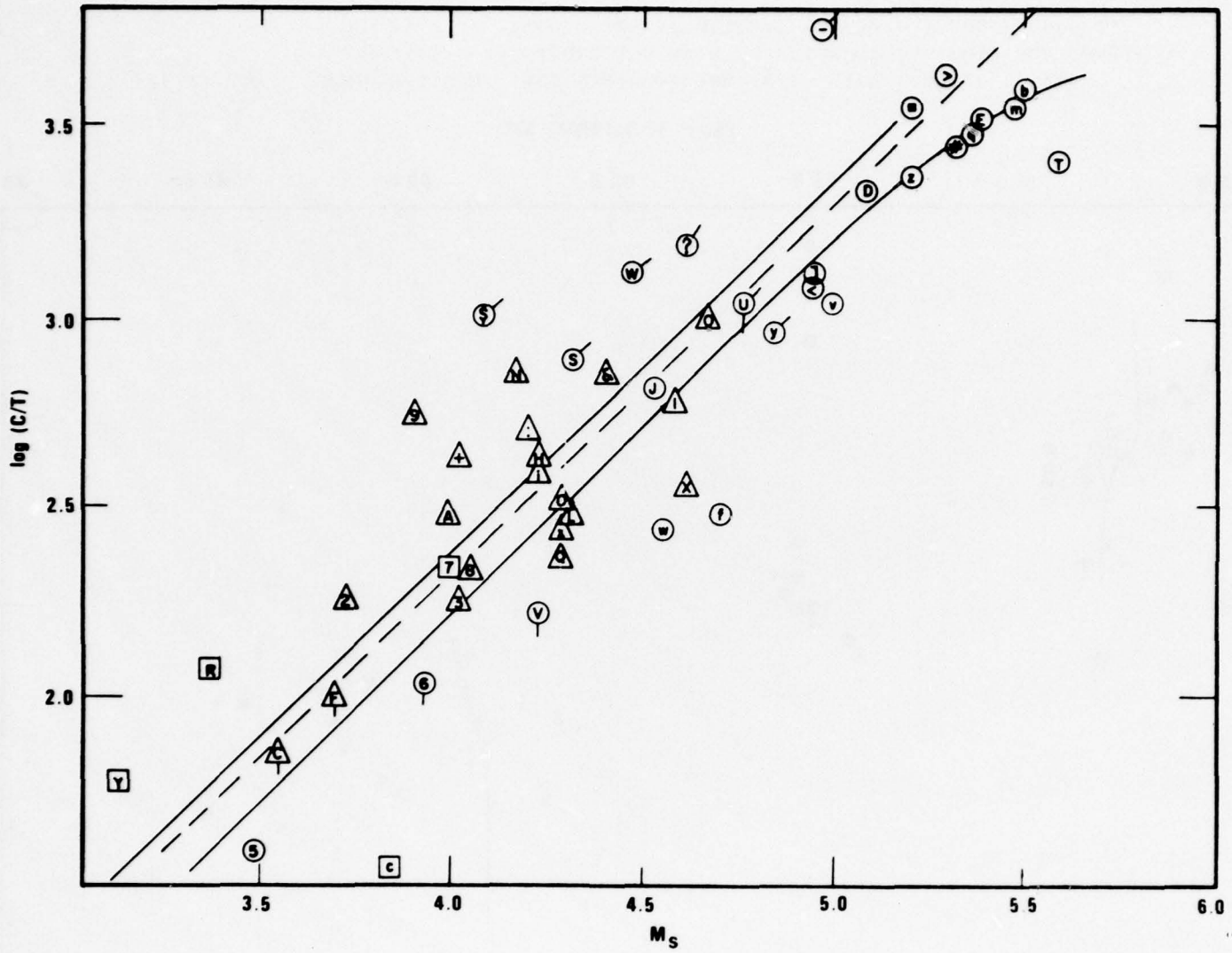

Figure 15a. HNME Station: Log (c/T), with c corrected for instrument response at period T, as a function of M_S. The dashed line is the least-squares line of slope 1.0 through all the data. The solid line is from Figure 3e with t* = 0.6, with the line vertically adjusted by eye so it best fits the data.

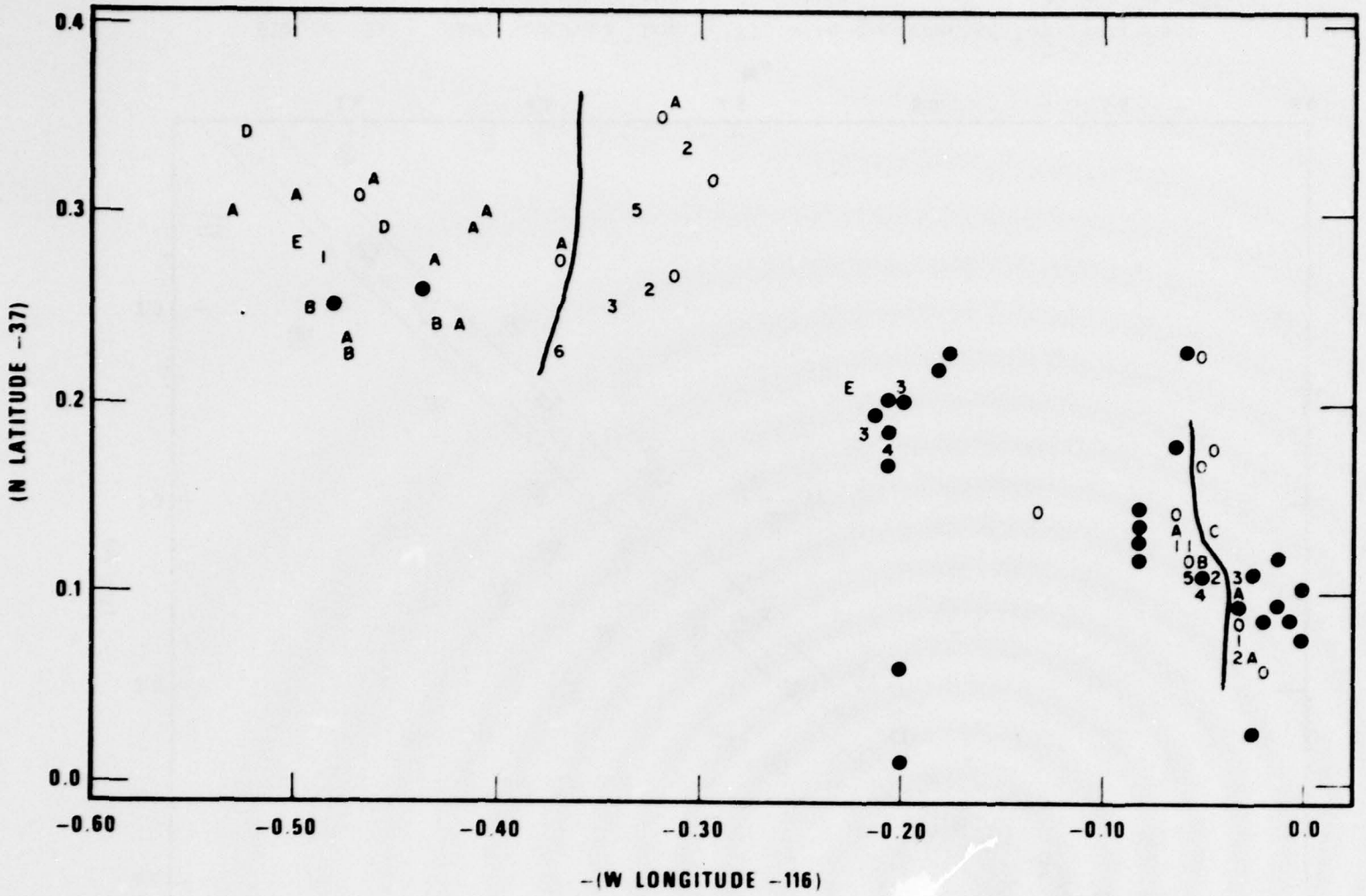

Figure 15b. HNME Station: Residuals of log (c/T) with respect to the dashed line in Figure 15a as a function of latitude and longitude at NTS. Events are identified in Table I and Figure 1.

SUMMARY AND DISCUSSION

In this report, von Seggern's (1976) near-equivalence of log(yield) and M_s has been used to show that both period and amplitude of short-period teleseismic body waves vary with yield, effects of pP, and geographic location. The variation from direct proportionality of amplitude versus log(yield) at megaton levels is on the order of 0.1 to 0.2 magnitude units, and the effects of pP have been shown to result in a spread of about 0.34 magnitude units. The variation with geographic region at an individual station is different for RKON and HNME, but a median value comparing west Pahute Mesa with Yucca Flats might be taken as 0.4 magnitude units.

The period varies from approximately 1.0 sec for a 5 kt explosion to 1.6 sec. for a 1000 kiloton. The period also shows a substantial variation due to pP effects and local geology. With these facts in mind, one would not expect it would be advisable to correct measured amplitudes for the system response at the measured period if all measurements were made on a common system. The problem is made worse, of course, if one considers that period measurements are notoriously difficult and that the signal is not monochromatic.

As reported in this study, magnitude and period effects of the size observed at single stations suggest that routine log(c/T) measurements cannot be adequate to the task of estimating seismic magnitude if a testing organization varies the depth of the events to an appreciable degree. Since the depth effect would be common to all stations in a network, the resulting bias could not be reduced by network averaging.

REFERENCES

Bakun, W.H., and L.R. Johnson, 1973, The deconvolution of teleseismic P waves from explosion MILROW and CANNIKIN, Geophys. J.R. Astr. Soc., v. 34, p. 321-342.

Blandford, R. R. (1976). Experimental determination of scaling laws for contained and cratering explosions; SDAC-TR-76-3, Teledyne Geotech, Alexandria, Virginia. DDC: ADA 03635.

Bogert, B.P., M.J.R. Healy, and J.W. Tukey, 1962, The frequency analysis of time series for echoes: ceptrum, pseudo-autocovariance, cross-ceptrum and phase-cracking, Proc. on Time Series Analysis, ed. M.

Der, Z. A. (1976). On the existence, magnitude and causes of broad regional variations in body-wave amplitude (magnitude bias); SDAC-TR-76-8, Teledyne Geotech, Alexandria, Virginia.

Der, Z. A., and T. McElfresh (1976). The effect of attenuation of the spectra of P waves from nuclear explosions in North America; SDAC-TR-76-7, Teledyne Geotech, Alexandria, Virginia. DDC: ADA 030857.

Fernald, A. T., G. S. Corchary, and W. P. Williams (1968). Surficial geologic map of Yucca Flats, Nye, and Lincoln counties; U.S. Geological Survey Map I-550.

Hinrichs, E. N. (1968). Geologic structure of Yucca Flats area, Nevada, in Geol. Soc. Am. Memoir 110, Nevada Test Site, edited by E. B. Eckel, Geological Society of America, Boulder, Colorado, p. 239-246.

Johnson, M. S., and D. E. Hibbard (1957). Geology of the Atomic Energy Commission Nevada Proving Grounds Area, Nevada; U.S. Geological Survey Bulletin 1021-K, U.S. Government Printing Office, Washington, DC.

Lyuke, E. I., S. K. Daragan, and V. E. Peregontseva (1976). Forecasting the seismic wave spectra of large underground detonations from the spectra of small preliminary detonations; Phys. Solid Earth (from Izvestiya), 12(2), 103-109.

Marshall, P. D., A. Douglas, and J. A. Hudson (1971). Surface waves from underground nuclear explosions; Nature, 234, 8-9.

Mueller, R. A., and J. R. Murphy (1971). Seismic characteristics of underground nuclear detonations: Part I, Seismic spectrum scaling; Bull. Seism. Soc. Am., 61, 1675-1692.

Noponen, I. (1975). Compressional wave power spectrum from seismic sources; Institute of Seismology, University of Helsinki, ISBN 951-45-0538-7, Contract AFOSR-72-2377 Final Report.

Orkild, P. P., K. A. Sargent, and R. P. Snyder (1969). Geologic map of Pahute Mesa Nevada Test Site and vicinity, Nye County, Nevada; U.S. Geological Survey Map I-567.

Ramspott, L. D., and N. W. Howard (1975). Average properties of nuclear test areas and media at the USERDA Nevada Test Site; UCRL-51948, Lawrence Livermore Laboratory, Livermore, California.

Rodean, H. C. (1972). Nuclear-Explosion Seismology; U.S. Atomic Energy Commission, Division of Technical Information, Oak Ridge, Tennessee.

Sargent, K. A., and P. P. Orkild (1973). Geologic map of the Wheelbarrow Peak-Ranier Mesa area, Nye County, Nevada; U.S. Geological Survey Map I-754.

Spence, W. (1974). P-wave residual differences and inferences on an upper mantle source for the Silent Canyon volcanic centre, Southern Great Basin, Nevada; Geophys. J. R. Astr. Soc., 38, 505-523.

Springer, D. L. and R. L. Kinnaman (1971). Seismic source summary for U.S. underground nuclear explosions, 1961-1970; Bull. Seism. Soc. Am., 61, 1073-1098.

Springer, D. L., and W. J. Hannon (1973). Amplitude-yield scaling for underground nuclear explosions; Bull. Seism. Soc. Am., 63, 477-500.

von Seggern, D. H., and R. R. Blandford (1972). Source time functions and spectra for underground nuclear explosions; Geophys. J. R. Astr. Soc., 31, 83-97.

von Seggern, D. H. (1973). Joint magnitude determination and analysis of variance for explosion magnitude estimates; Bull. Seism. Soc. Am., 63, 827-845.

von Seggern, D. H. (1976). M_S versus yield of underground nuclear explosions at the Nevada Test Site; SDAC-TR-76-11, Teledyne Geotech, Alexandria, Virginia.

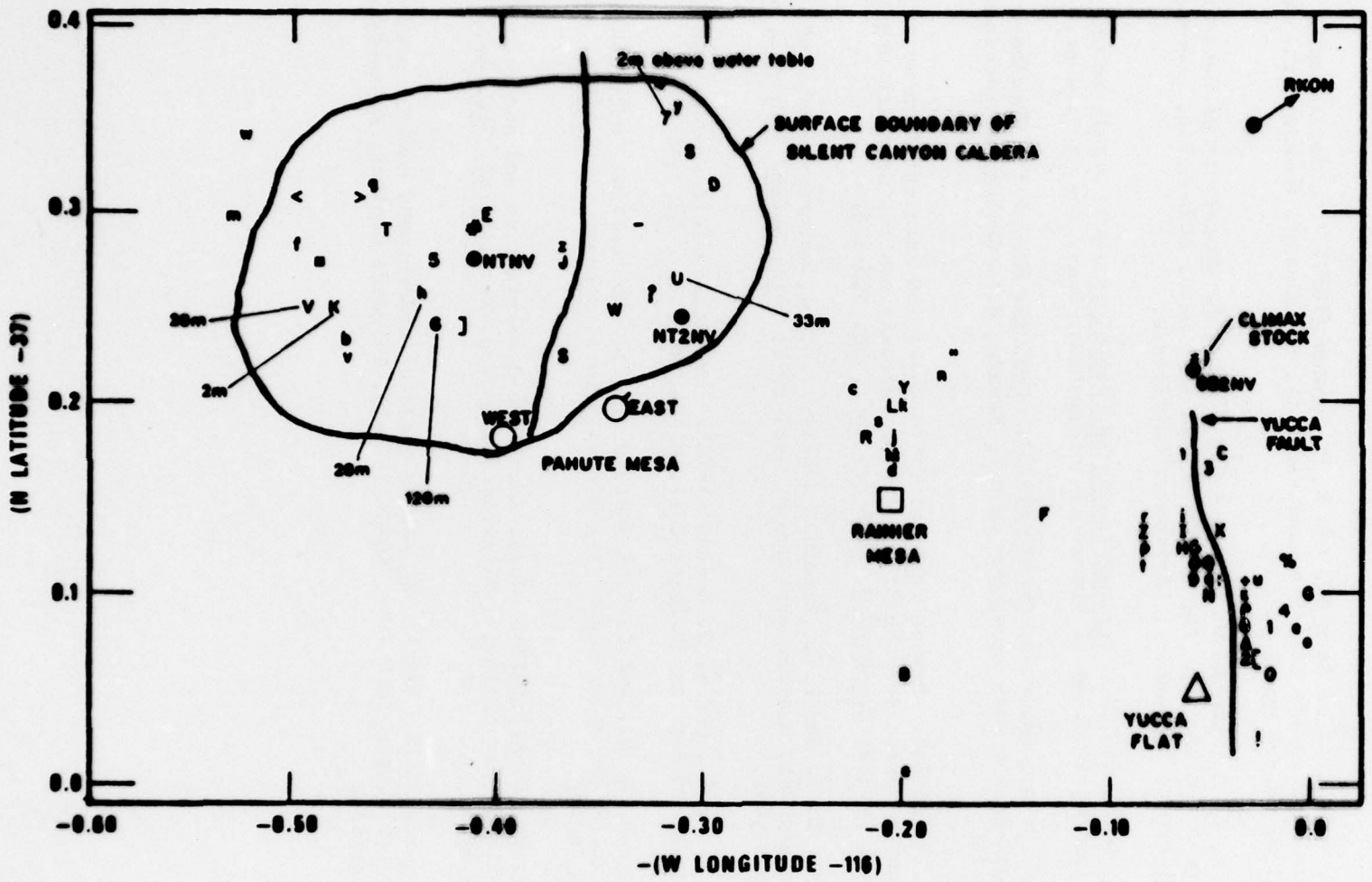
2m above water table
SURFACE BOUNDARY OF
SILENT CANYON CALDERA
RKON
NTNV
NT2NV
28m
2m
33m
28m
120m
WEST
EAST
PAHUTE MESA
RANIER
MESA
CLIMAX
STOCK
YUCCA
FAULT
YUCCA
FLAT
(N LATITUDE -37)
-(W LONGITUDE -116)
0.4
0.3
0.2
0.1
0.0
-0.60
-0.50
-0.40
-0.30
-0.20
-0.10
0.0